Tunability of Physical Properties of $Zn_{1-x}Cu_xSe$ Nano Crystalline Thin Films With Copper Concentration and Ion Beam Analysis by Rutherford Backscattering Spectroscopy

By

Muhammad Arslan

Thesis submitted to the School of Chemical and Materials Engineering (SCME) in partial fulfillment of requirements for the Degree of MS Materials Engineering

SCHOOL OF CHEMICAL AND MATERIALS ENGINEERING

NATIONAL UNIVERSITY OF SCIENCES AND TECHNOLOGY

H-12, ISLAMABAD PAKISTAN

Declaration of Originality

I hereby declare that the work contained in this thesis and the intellectual content of this thesis are the product of my own work. This thesis has not been previously published in any form nor does it contain any verbatim of the published resources which could be treated as infringement of the international copyright law.

I also declare that I do understand the terms ‘copyright’ and ‘plagiarism,’ and that in case of any copyright violation or plagiarism found in this work, I will be held fully responsible of the consequences of any such violation.

Signature: _____

Name: Muhammad Arslan

Date: _____

Place: NUST H-12, ISLAMABAD

Certificate of Approval

This is to certify that the work contained in this thesis entitled

"Tunability of Physical Properties of $Zn_{1-x}Cu_xSe$ Nano Crystalline Thin Films With Copper Concentration and Ion Beam Analysis by Rutherford Backscattering Spectroscopy"

Is carried out by

Muhammad Arslan

Under our supervision and that in our opinion, it is fully adequate, in scope and quality, for the degree of MS (Materials Engineering) from National University of Sciences and Technology (NUST)

Approved By:

Signature: _____

Supervisor: ***Dr. Amir Habib***

Signature: _____

CO-Supervisor: ***Dr. Muhammad Shahid***

Verified By:

Signature: _____

Head of Department (Materials Engineering)

Dedicated to my dear parents

who have always been so close to me

that I found them nearest to me whenever I needed.

It is their unconditional love that has always been a source of strength for me &

which motivates me to set higher targets.

Acknowledgement

All prays and glory is due to **ALLAH**, Whose worth cannot be described even by the greatest rhetoricians of all times, Whose blessings and bounties cannot be enumerated by beckoners and enumerators of all ages, and homage due to Him cannot be adequately paid even by the most assiduous and revering attempters.

It is my privilege to express my deep sense of gratitude to my research **supervisor**, **Dr. Amir Habib**, for his constant persuasion, affectionate guidance and efficient supervision at each and every stage of this research work.

I would like to express my special thanks to **Prof Dr Muhammad Shahid** (HOD Materials engineering SCME**)** whose invaluable guidance, remarkable suggestions, constant encouragement, constructive criticism and cooperation during my project work has been of great help to me in this research work.

I greatly acknowledge **Prof Dr Mohammad Mujahid** (Principal School of Chemical and Materials Engineering SCME) for providing a platform to utilize my skills in the research work. I would like to thank all the faculty members nonteaching staff and my fellow students for the help provided to me at various stages during this research work

My sincere thanks are to **Dr Ghulam Husnain** (senior scientist, National center for physics QAU) for their constant motivation support and cooperation during the period of my research work.

M. Arslan

Table of Contents

List of figures

Figure 4.8: AFM 2-D and 3-D images of 400ºC annealed (a) x= 0.00 and (b) 0.10 thin films

Figure 4.9: Curve fitting of psi and delta by Ellipsometry

Figure 4.10: Band gap energy of as-deposited and annealed (200ºC and 400ºC) $Zn_{1-x}Cu_xSe$ (a) x= 0.00, (b) x= 0.05, (c) x= 0.15 films, determined from k-spectra. Inset in Fig. 4.10c shows the variations of band gap energy of as-deposited and annealed (200ºC and 400ºC) $Zn_{1-x}Cu_xSe$ films with copper concentration.

Figure 4.11: Dielectric constant (ε_1) of as-deposited and annealed $Zn_{1-x}Cu_xSe$ (a) x=0.00 (b) x=0.05, (c) x=0.20 films, determined by spectroscopic ellipsometer. Inset in Fig. 4.11c shows the variations of dielectric constant of as-deposited and annealed (200ºC and 400ºC) $Zn_{1-x}Cu_xSe$ films with copper concentration at λ=550 nm.

List of tables

Abstract

The accurate composition and concentration depth information of the as-deposited and annealed $Zn_{1-x}Cu_xSe$ films were recorded by Rutherford backscattering spectroscopy (RBS) technique. The films were grown on simple glass substrates by using close spaced sublimation technique. Precursor films, having thickness of about 250 to 300 nm, were afterward annealed in air atmosphere at temperatures of 200ºC and 400ºC for 1 hour. Structural characterization including crystal structure and orientation, stacking fault energy and surface morphology were calculated by using X-ray diffraction (XRD) and atomic force microscopy (AFM). Characterization of optical properties such as absorption coefficient, band gap energy estimation and dielectric constant was done by spectroscopic ellipsometer. A comparison of XRD results revealed that as-deposited and annealed films have polycrystalline nature with zinc-blende structure in the (111) plane. Stacking fault energy (SFE) of the films determined from XRD data decreases with increasing annealing temperature and also decreases by increasing Cu concentration up to 10% and then increases for 15% and 20% Cu concentration. AFM studies revealed that surface morphology is enhanced with increasing annealing temperature of 400ºC. The band gap energy of the films determined using *k* spectra by spectroscopic ellipsometer increases while dielectric constant decreases with increasing annealing temperature.

CHAPTER 1

1 INTRODUCTION

This project has been accomplished with an aim to study the physical properties of $Zn_{1-x}Cu_xSe$ films deposited by closed space sublimation technique. The concentration of copper has been varied and effect of post annealing temperature is studied in detail. These altered properties have been investigated by concentration depth profiles determined by Rutherford backscattering spectroscopy (RBS) technique. This method has been used to find out the composition, film thickness, stoichiometry and concentration depth profiles in semiconductors and metal thin films. Various applications of the Rutherford backscattering spectroscopy have been discussed. Extensive discussion based upon electronic interaction where scientists involved in this phenomenon can exchange and discuss ideas, information and new scientific concepts. Various other structural and optical properties of the prepared nano crystalline $Zn_{1-x}Cu_xSe$ thin films have also been investigated.

1.1 Thin Film Technology

Thin film is a very thin layer with an exceptional high surface-to-volume ratio. These are the layers of materials varying from fractions of a nanometer to more than a few microns in thickness. Films are considered as thin, if we can create the surface properties with the purpose of markedly different properties from the bulk. In thin films, the forces which are acting on the surface atoms are totally dissimilar from those of the bulk. The reliability of thin films is subjected to the quality of its adhesion with the substrate, any residual or intrinsic stresses after the deposition, or the occurrence of surface defects or impurities. A film that peels off when the device is subjected to thermal or mechanical stresses can results in device failure. This adhesion depends mainly on the cleanliness of the substrate surface. A very smooth or rough substrate roughness also affects thin film adhesion.

There are always some intrinsic stresses while fabricating the thin films, irrespective of the deposition process. These stresses can either be compressive or tensile and can lead to adhesion tribulations, cracking and corrosion. Therefore, optimum deposition conditions are critical to minimize intrinsic stresses in the films [1]. Microelectronics is still one of the important fields in which thin film technology is being used. However, there are other rising and expanding applications in areas like magnetic and optical devices, shielding and nano-materials coatings [2]. Previously thin films have been engaged in making electronic devices and optical coatings etc. Now this significant technology is being developed in the twenty-first century for the development of a new material such as nano-materials. The processing of thin films is also an energy saving process for the production of the devices [3].

1.2 Importance of Thin Films

The thin films significance becomes more important when there is a need to generate the conflicting or enhanced properties in a material that frequently are inconsistent in nature if we use a standardized one. Some applications require properties which occupy different features at the surface than those of the bulk. E.g. the operation of ICs depends on the electrical charges and the interface between dissimilar materials with diverse electronic properties. The desired properties of a composite material can be attained by producing it as bulk material and then coating a thin film on its surface. In the fabrication of lasers, geometrical and structural requirements are obtained by sandwiching different semiconductors in the form of films. Thin films also provide suitable coatings to enhance the effectiveness and extend the lifetime of the high temperature materials.

There are other various appliances where the exclusivity of thin films is important to the observed performance. Examples include: giant-magneto resistance films, thin film superconductors, super-lattice films and hetero structure lasers, etc [4, 5]. Micro-electromechanical systems (MEMS) are devised to operate as sensors and actuators [6]. Thin film deposition systems are merely accessible technique for coating of lenses and mirrors, also optical integrated circuits and micro-mechanical device manufacturing needs this particular technology for their implementation [7].

1.3 Thin Film Deposition

Thin film deposition involve four major stages

1. Create vapor phase.
2. Convey atoms/molecules from the target material to the surface of the substrate.
3. Deposition of atoms/ molecules on the substrate surface.
4. Rearranging of atoms/molecules of the deposited film to attain the preferred properties.

The first stage contains all the methods which are essential for the creation of the vapor phase from the condensed state. Some typical methods are the thermal evaporation, e-beam evaporation, sputtering etc. In the second stage the atoms in the form of vapors are transported from the target material and adsorbed on to the substrate. Some techniques such as electron cyclotron resonance plasma assisted growth and activated reactive evaporation are used to control the motion of the evaporated species before they deposit onto the substrate. In the third stage, the evaporated atoms are deposited on the substrate. Epitaxial growth of the films is a major area of thin film technology which is concerned to give a sole control on the composition, structure and defect free growth of the film. In the fourth stage, the rearranging of the atoms or reconfiguring the surface morphology of the film takes place to give the preferred properties for the product. Formation of a thin film begins via nucleation and growth processes [7]. Step-by-step growth process can be presented as follows:

The vapors on impacting the substrate surface lose their normal component of velocity and are adsorbed onto the substrate surface. Initially the adsorbed atoms being not in thermal equilibrium with the substrate keeps on changing their position over the substrate surface. The adsorbed atoms interact among themselves, forming bigger nuclei. These appearing nuclei are thermodynamically unstable and have a tendency to desorb. If the deposition factors are controlled in an optimum manner such that other adsorbed species collides with nuclei prior to getting desorbed, it begins to grow in size. After attaining a confident critical size, the nuclei become thermodynamically stable and this step is called the nucleation stage. A number of critical nuclei grow in reasonable dimension until a saturation point of highest nucleation density is achieved. The nucleation density and the size of nuclei depend on a number of factors such as

the activation energy of the adsorbed species, substrate temperature, the rate of impingement and chemical/physical nature of the substrate. Nuclei can grow on the substrate in two ways: either by diffusion of the adsorbed species parallel to the surface of substrate by or perpendicular to it by direct collision of the incoming species. The grown-up and mature nuclei are called islands.

In the next stage, these formed islands start coalescing with each other to decrease the substrate surface area in the progression of film formation. At this stage the formation of bigger islands is enhanced by increasing the substrate temperature thus increasing the surface mobility of the adsorbed species and agglomeration is assumed to happen. [8].

1.4 Thin Film Deposition Techniques

In most of the literature, generally the formation of thin films is classified into two main categories

1. Chemical vapor Deposition (CVD)
2. Physical Vapor Deposition (PVD)

In chemical vapor deposition, the film composition varies from that of the target material whereas, in physical vapor deposition the deposited material is said to have the similar composition as the source. In general, physical deposition methods are very common either regarding the material to be deposited or to the particular substrate. There are many techniques that use the combination of both. A list of different techniques is given below.

1.4.1 Chemical Vapor Deposition

Here, a precursor in fluid form goes through a chemical change at the substrate surface, parting a solid layer. The fluid tends to surround the solid film, deposition occurs on the surface, with a very minute consideration to direction. Thin films deposited by CVD techniques tend to be *conformal*, rather than *directional*. CVD normally uses a gas precursor, generally a hydride or halide of the material to be fabricated. In MOCVD, metal-organic gas is used. Some of the commonly used CVD techniques are:

a) Plasma enhanced (PE) CVD

b) Plasma polymerization

c) Chemical vapor deposition (CVD)

d) Chemical solution deposition (CSD)

1.4.2 Physical Vapor Deposition

Physical vapor deposition utilizes mechanical ways to fabricate a thin film of target material. The target material is positioned in an energetic and high vacuum chamber so that vapors of material can escape the surface. The whole deposition process is done in a vacuum environment, to permit the particles to travel without any restriction. In this way, the vapors follow a straight path and the deposited films are *directional*.

PVD has three fundamental steps to deposit a thin film. First solid target material is sublimated to vapors; Secondly, atoms in vapor state passes through the vacuum to the substrate surface. Lastly, target material is deposited onto the substrate surface to produce an optical thin film. Some of the commonly used PVD techniques are:

a) Sputtering
b) Pulsed Laser Deposition (PLD)
c) Molecular Beam Epitaxy (MBE)
d) Thermal Evaporation

The technique which I have used to deposit the films is close spaced sublimation technique. It is one of the types of thermal evaporation technique so we concentrate on this particular technique.

1.4.3 Close spaced sublimation (CSS)

Close spaced sublimation (CSS) is a type of thermal evaporation. It is an old PVD technique commonly used for coating technology in decorations and wear resistance applications [12]. In this technique the target material is placed in a boat of resistive element such as tungsten, molybdenum and tantalum etc. Some of the resistive element boats are shown in the Fig. 1.1. A very high direct current is allowed to pass in these boats with very low voltage. The melting point of resistive boats is very higher than the target materials, therefore the material is evaporated and deposited on the substrate surface by producing joule heating effect. The target material and substrate are closely spaced usually just a few mm apart. The target material can be

of any shape as you have demand.CSS is widely used in the manufacturing of microelectronics and in the research labs making the most efficient II-VI compound semiconductor solar cells.

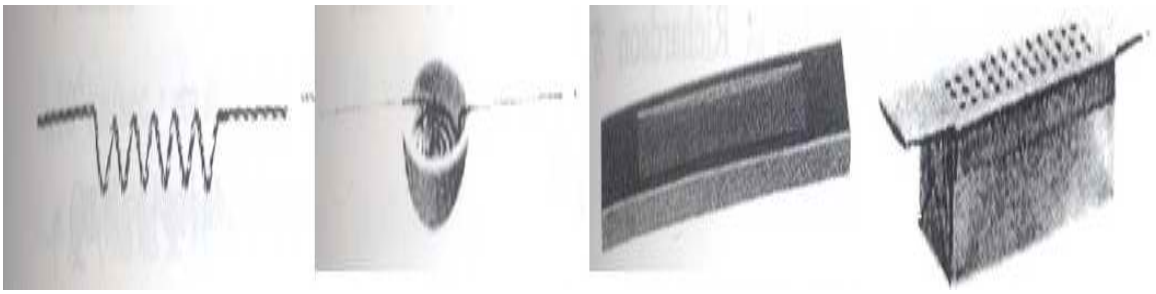

Fig. 1.1: Different types of resistive elements [5]

1.5 Introduction to Material

$Zn_{1-x}Cu_xSe$ is a ternary alloy of Zinc, Copper and Selenium. Zinc and copper belongs to group-II of periodic table while selenium belongs to group VI. Therefore $Zn_{1-x}Cu_xSe$ is known as II-VI compound semiconductor. In recent years, it got much more attraction in semiconductor technology because of superb optical properties [13-20]. It is widely used in optoelectronics, solid state devices and solar cells. Its energy band gap as well as lattice parameter can be varied linearly with x. The band gap of this material may varies by adding Copper content in ZnSe binary compound semiconductor. ZnSe has high band gap energy of the order ~ 2.7eV at room temperature.

This work consists of two phases: In the first phase we have prepared series of solid solution of $Zn_{1-x}Cu_xSe$ ($0.00 \leq x \leq 0.20$) by physical mixing and then its thin films were grown on a BK-7 glass substrate by using close spaced sublimation technique. The deposited films were also annealed at 200^oC and 400^oC temperature in air for 1 hour. In the second phase these as-deposited and annealed samples were characterized by using different diagnostic tools. For compositional analysis Rutherford backscattering spectroscopy (RBS) has been employed. X-ray diffraction (XRD) and atomic force microscopy (AFM) were utilized for the structural analysis whereas for optical analysis spectroscopic ellipsometer was used.

1.6 Zinc Selenide

Zinc Selenide is a chemical compound of II-VI group of periodic table. The color of ZnSe is light yellow and is a direct band gap compound binary semiconductor. The band gap value is 2.7eV at 300K temperature. ZnSe occurs naturally in the mineral stilleite with cubic zinc blende structure. Molar mass of ZnSe is 144.35g/mol, Density is 5.27 g/cm^3, Melting point is 1525 °C while Refractive index is 2.67 at 550nm.

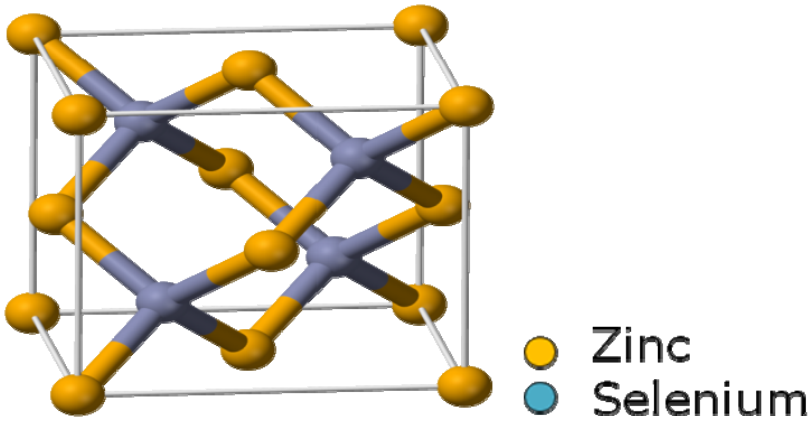

Fig. 1.2: Zinc-blend structure of Zinc Selenide

ZnSe is used to form semiconducting LEDs and diode lasers [21]. It is susceptible to n-type and P-type doping with group VII and nitrogen elements respectively. It has a refractive index of about ~ 2.67 at 550 nm and has amazingly broad transmission wavelength range (0.45 µm to 21.5 µm) hence used as an infrared optical material [22]. Chromium doped ZnSe (**ZnSe:Cr**) is used as an infrared emitting laser which operates at ~ 2.5 µm [23]. ZnSe is shaped as micro crystalline sheets by synthesis from H_2Se gas and Zn vapors. ZnSe enriched with tellurium (ZnSe:Te) is a scintillator [24] and can be synchronized with photodiodes with an emission peak ~ 640 nm. It is also used in CO_2 laser lenses, X-ray and gamma ray detectors, ATR prisms, night vision appliances, and transmission windows for IR spectroscopy [25].

1.7 Copper

Copper (Cu) is a chemical element with atomic number 29 and electronic configuration given by [Ar] $3d^{10}$ $4s^1$. Pure Cu has reddish-orange color and is slightly soft and flexible. It is a

ductile metal with incredibly high thermal and electrical conductivity. It is used as a construction material, and essential component of different metal alloys. Cu compounds are generally found as salts of Cu^{2+} and have been used in the past extensively as pigments. Cu in cooperation as metal or pigmented salt has a key existence in decorative art. Cu metal architectural structures and statuary corrodes in due course to attain a characteristic green glaze.

Table 1.1: Some physical properties of Copper

Atomic radius	Electro-negativity	Boiling point	Melting point	Density	Crystal structure	Electrical resistivity	Hardness Mohs
1247.8pm	1.9	2562°C	1084.6°C	8.94 $g \cdot cm^{-3}$	F.C.C	16.78 $n\Omega \cdot m$	3.0

1.8 Thesis Motivation and Objective

The motivation regarding to my work is totally based on experimental work related to the compositional, structural and optical characteristics of $Zn_{1-x}Cu_xSe$ thin films with different Cu concentration. A number of researchers carried out enormous research work on ZnSe to examine the effects of Cu doping on different properties (structural, optical and electrical) by means of various synthesis and characterization techniques.

The core purpose of this research work is to study compositional, structural and optical properties in $Zn_{1-x}Cu_xSe$ thin films enriched with Cu. Copper creates acceptors levels which can be used in the optical processing. Cu levels are in the 0.68 eV energy depth range corresponding to the wavelength range of optical telecommunications [26]. Here we have motive that up to which extent Cu concentration affects crystal lattice, optical properties and crystalline quality of host material. Due to compositional and crystal changes whether we observe amorphous or semi crystalline character? Finally by process of subsequent post annealing after the deposition of films, how much we recover lattice damages/disorder in order to improve surface, structure and crystalline quality of the deposited $Zn_{1-x}Cu_xSe$ thin films. For this reason my concentration throughout this dissertation is obviously on investigation of compositional, structural and optical properties of Cu enriched $Zn_{1-x}Cu_xSe$ thin films.

1.9 References

1. www.Siliconfareast.com/Thin_films_Semiconductor_manufacturing.
2. K. S Sree Harsha. Principls of physical vapor deposition. Elsevier (2006).
3. K. Wasa, M. Kitabatake, H. Adachi. Thin film material technology, sputtering of compound materials. Springer. William Andrew (2004).
4. K. S. Sree Harsha. Principles of Vapor Deposition of Thin Films (2006).
5. Kiyotaka Wasa. Thin film technology as a materials engineering. Revista Brasileira de Aplicacoes de Vacuo. **20** (2001).
6. S. Trolier-Mckinstry, P. Muralt. Thin Film Piezoelectrics for MEMS. Journal of Electroceramics **12** (2004) 7-17.
7. M. Ohring. The material science of thin films. San Diego New York (1992).
8. ETAFILM Technology. www.etafilm.com.tw. Chungli Ciy. Taoyuan Hsien 320. Taiwan.
9. Christopher B Ebert, Loren A Eyres, Martin M Fejer, James S Harris Jr.. MBE growth of antiphase GaAs films using GaAs/Ge/GaAs heteroepitaxy, Journal of Crystal Growth **201–202** (1999) 187–193.
10. Torsten Rieger, Sonja Heiderich, Steffi Lenk, Mihail Ion Lepsa, Detlev Grützmacher, Ga-assisted MBE growth of GaAs nanowires using thin HSQ layer. Journal of Crystal Growth**. 353** (2012) 39-4.
11. Osamu Morohara, Hirotaka Geka, Yoshitaka Moriyasu, Naohiro Kuze. Sb irradiation effect on growth of GaAs thin film on Si (111) substrate. Journal of Crystal Growth**, 378** (2013) 113-116.
12. Marc J. Madou. Fundamentals of Microfabrication: The Science of Miniaturization, 2nd Ed. (2002).
13. O. Schulz, M. Strassburg, T. Rissom, U.W. Pohl, D. Bimberg. Post-growth *p*-type doping enhancement for ZnSe-based lasers using a Li_3N interlayer. Appl. Phys. Lett. **81** (2002) 4916.
14. P. Mahawela, G. Sivaraman, S. Jeedigunta, J. Gaduputi, M. Ramalingam, S. Subramanian. II–VI compounds as the top absorbers in tandem solar cell structures. Mater. Sci. Eng. B **116** (2005) 283.

15. P. K. Kalita, B. K. Sarma, H. L. Das. Structural characterization of vacuum evaporated ZnSe thin films. Bull. Mater. Sci. **23** (2000) 313.

16. S. Venkatachalam, S. Agilan, D. Mangalaraj, S. K. Narayandass. Optoelectronic properties of ZnSe thin films. Mater. Sci. Semicon. Proc. **10** (2007) 128.

17. Xiaojun Zhang, Kin Man Yu, Coleman X. Kronawitter, Zhixun Ma, Peter Y. Yu, andSamuel S. Mao. Heavy p-type doping of ZnSe thin films using Cu_2Se in pulsed laser deposition. Appl. Phys. Lett. **101** (2012) 042107.

18. T. Shi rakawa. Effect of defects on the degradation of ZnSe-based white LEDs. Mater. Sci. Eng. B **91-92** (2002) 470.

19. M. Godlewski, E. Guziewicz, K. Kooalko, E. Lusakowska, E. Dynowska, M. M. Godlewski, E. M. Godys, M. R. Phillips. Origin of white color light emission in ALE-grown ZnSe. J. Lumin. **102–103** (2003) 455.

20. M. Drechsler, B. K. Meyer, D. M. Hofmann, P. Ruppert, D. Hommel. Optically detected cyclotron resonance properties of high purity ZnSe epitaxial layers grown on GaAs. Appl. Phys. Lett. **71** (1997) 1116.

21. G. Landwehr and D. Hommel. Blue-Green ZnSe Laser Diodes for Optoelectronics. physica status solidi (b) **187** (2006).

22. www.kayelaby.npl.co.uk/general physics.

23. G. Grebe, G. Roussos, H.-J. Schulz. C^{r2+} excitation levels in ZnSe and ZnS. J. Phys. C: Solid State Phys. **9** (1976) 4511-4516.

24. V. D. Ryzhikov, N. G. Starzhinskiy, L. P. Gal'chinetskii, L. L. Nagomaya, P. A. Gashiu, V. P. Makhniy, G. Tamulaitis, W. Klamra, D. N. Kozin, E. A. Danshin. Properties of semiconductor scintillators ZnSe(Te,O) and integrated scintielectronic radiation detectors based thereon. Nuclear Science Symposium Conference Record **1** (2000). DOI. 10.1109/NSSMIC.2000.949152

25. www.internationalcrystal.net/optics.

26. M. Godlewski, W.E. Lamb, B.C. Cavenett. ODMR investigations of recombination processes in ZnSe:Cu. Solid State Comm. **39** (1981) 595–599.

CHAPTER 2

2 LITERATURE SURVEY

In order to achieve improved and optimum physical properties, extensive works have been carried out on the synthesis and characterization of Cu-doped ZnSe thin films using different deposition techniques and Cu contents [1-7]. According to our knowledge, very little is reported for doping of higher Cu concentrations in ZnSe films prepared by closed space sublimation technique. In this regards, an effort has been made to prepare $Cu_xZn_{1-x}Se$ thin films by closed space sublimation technique which is more common, economical and conventionally simple process. Some of the structural and optical features of as-deposited and annealed $Zn_{1-x}Cu_xSe$ films have already been published in our recent articles [8, 9].

In 2005, Zulfiqar Ali [10] prepared ZnSe thin films using two sourced evaporation technique. Evaporation rates of both Zn and Se were controlled at substrate temperature of 400^oC. The films were enriched with Cu by dipping in $CuNO_3.2H_2O$ solution for different tenures of time. It was found that the as-deposited films were polycrystalline in nature having FCC zinc-blende structure grown along (111) plane. The films which were treated by $CuNO_3.2H_2O$ solution and annealed were less oriented in [111] plane. No peak corresponding to Cu compound come into sight for post treated films which might be due to the very less quantity of Cu in the films. Grain size was determined using scherrer formula and found that it is of the order of 25 nm. Band gap energy decreases with increasing Cu content while refractive index increases. The resistivity of the as-deposited films fall from 10^9 Ω-cm to about 1.6 Ω-cm for $CuNO_3.2H_2O$ solution treated films after annealing in vacuum.

In 2008, K. R. Murali [11] deposited ZnSe thin films with varying deposition temperatures in the range of 30-80 ^0C by using pulse plating technique. The films were on deposited onto titanium and conducting glass substrates at 50% duty cycle. The as-deposited films were doped with copper by immersing them in 0.01 M concentrated Cu_2NO_3 solutions. Amount of doped Cu in ZnSe films were estimated by dissolving them in aqua regia which

showed that the Cu concentration increases from 0.001-0.009 ppm. The films reveal cubic structure with multi-peaks corresponding to the (111), (220) and (311) reflections. As the duty cycle raises the intensity of the (111) peak increased, indicating the preferential growth in (111) plane. Broad peaks become sharper as the deposition temperature increases which is merely due to the enhanced crystallinity. The band gap energy (E_g) was estimated in the range of 2.64-2.68 eV which showed that E_g increases with the rise in deposition temperatures. Surface morphology of the films was imaged by AFM and it was noticed that the RMS value increased from 43-76 nm as the deposition temperature increases. These are similar to the results acquired with photo chemically deposited ZnSe films [12].

In 2001, Encai Hao [13] reported the formation of ZnSe and Copper doped ZnSe nano-particles synthesized using layer-by-layer assembly. Using cationic and anionic alternating polymer layers, Cu-doped ZnSe nano-particles were assembled into composite ultrathin films. The surface conditions and dimensions of doped ZnSe nano-particles were controlled and characterized using UV-Visible, fluorescence and XPS methods. These characterization techniques confirmed the presence of Cu-doped ZnSe in the polymer films. The synthesized nano-particles showed strong blue light emission.

In 2007, Masahiro Orita [14] prepared Cu doped ZnSe crystalline films on glass substrates from ZnSe and Cu_2Se powders using the evaporation method. Post annealing treatment at 400^{o}C in a vacuum improved the crystallinity and no secondary phase was observed using X-ray diffraction for a film with a Cu concentration of 0.10%, which had a conductivity of 28 S-cm^{-1} and good transparency at green and red wavelengths. The thermal probe test indicated p-type carrier polarity and the effects of annealing were confirmed by irradiating the as-deposited films with a YAG laser 355 nm. Possibility of producing transparent p-type conducting films on polymer substrates is demonstrated.

Our recently published article in journal of Acta Metallurgica Sinica (2013) describes the preparation of the same as-deposited and annealed (200^{o}C and 400^{o}C) $Zn_{1-x}Cu_xSe$ thin films by CSS technique [9]. Effect of thermal annealing on the structural, optical and vibrational properties of the deposited films were investigated using analytical tools RBS, XRD, spectrophotometer and spectroscopic ellipsometry. By increasing the annealing temperature of films from 200^{o}C to 400^{o}C the physical properties have improved significantly which shows that

the annealing effect is very prominent in the properties of thin films. XRD data predict the improvement of the crystallinity and increase in the grain size with the increase of the annealing temperature. Strain (ε) and dislocation density (δ) were also measured by XRD parameters. It was observed that strain and the dislocation density decreases with increasing annealing temperature. The decreasing trends of strain and dislocation density with annealing temperature are due to the enhancement of crystallization. Spectrophotometer data verified that the optical transmittance as well as the band gap increased with the increase in annealing temperature. The band gap was determined using the Tauc's relation. Spectroscopic ellipsometry analysis revealed that the optical constants i.e. refractive index & extinction coefficient decreases with the increase in the annealing temperature. Moreover thickness decreases with increasing temperature which was also confirmed by spectroscopic ellipsometry and Rutherford backscattering spectroscopy.

In the present work we have investigated the compositional, structural and optical results in a different way regarding lattice parameters, surface roughness, and band gap tune-ability by using *k* spectra through spectroscopic ellipsometry for optoelectronic applications. Additionally, the new findings in this work are the detailed analysis of the effect of post deposition thermal annealing on the depth concentration of deposited layers of $Zn_{1-x}Cu_xSe$ thin films by RBS technique. Variations in stoichiometry found with RBS technique is complemented by micro analysis characterization performed by XRD, AFM and the optical property results obtained using spectroscopic ellipsometer. Complete correlation between experimentally derived results and their technically important properties has been discussed. The results obtained show that the films are of potential significance for obtaining optimum quality films particular for device fabrication.

2.1 References

1. M. El Sherif, F. S. Terra, S. A. Khodier. Optical characteristics of thin ZnSe films of different thicknesses. J. Mater. Sci, Mater. Electron. **7** (1996) 391.
2. S. Venkatachalam, D. Mangalaraj, Sa. K. Narayandass, K. Kim, J. Yi. Structure, optical and electrical properties of ZnSe thin films. Physica B **358** (2005) 27.
3. R. F. Bunshah. Handbook of Deposition Technologies for Films and Coatings, 2nd ed, Noyes Publications, New Jersey, 1994.

4. N. Xu, Z. F. Ying, Y. C. Du, F. M. Li. Pulsed laser deposition of ZnSe:N epilayers assisted by active atomic nitrogen beams. Curr. Appl. Phys. **1** (2001) 209.
5. T. Ganguli, M. Vedvyas, P. Bhattacharya, L. M. Kukreja, A. Ingale, K. P. Adhi, K. S. Chandrashekharan, B. M. Arora, K. C. Rustagi. Crystalline quality of ZnSe thin films grown on GaAs by pulsed laser deposition in He and Ar ambient. Thin Solid Films **388** (2001) 189.
6. S. D. Setzler, M. Moldovan, Z. Yu, T. H. Myers, N. C. Giles, L. E. Halliburton. Observation of singly ionized selenium vacancies in ZnSe grown by molecular beam epitaxy. Appl. Phys. Lett. **70** (1997) 2274.
7. D. Wolverson, P. J. Boyce, C. M. Townsley, B. Schlichtherle, J. J. Davies. Spin-flip Raman scattering studies of doped epitaxial zinc selenide. J. Cryst. Growth **159** (1996) 229–37.
8. M. Arslan, A. Maqsood, A. Mahmood, A. Iqbal. Structural and optical properties of copper enriched ZnSe thin films prepared by closed space sublimation technique. Mat. Sci. Semicond. Proc. **16** (2013) 1797–1803.
9. M. Arslan, R. Muhammad, A. Mahmood, R. Rasheed. Effect of thermal annealing on the physical properties of $Zn_{1-x}Cu_xSe$ thin films deposited by close spaced sublimation technique. Acta Metall. Sin. (Engl. Lett.) (2013) **26** 699-706.
10. Z. Ali, A. K. S. Aqili, A. Maqsood. Properties of cu-doped low resistive ZnSe films deposited by two-sourced evaporation. Vacuum **80** (2005) 302–309.
11. K. R. Murali. Properties of ZnSe films pulse plated on high temperature substrates. Chalcogenide Letters **5** (2008) 111–116 .
12. R. Kumaresan, M. Ichimura, E. Arai. Photochemical deposition of ZnSe polycrystalline thin films and their characterization. Thin solid films **414** (2002) 25-30.
13. E. Hao, H. Zhang, B. Yang, H. Ren. J. Shen. Preparation of Luminescent Polyelectrolyte/Cu-Doped ZnSe Nanoparticle Multilayer Composite Films. J. Colloid and Interface Science **238** (2001) 285-290.
14. M. Orita, T. Narushima, H. Yanagita. Transparent Conductive Cu-doped ZnSe Film Deposited at Room Temperature Using Compound Sources Followed by Laser Annealing. Jap. J. Appl. Phys. **46** (2007) L976-L978.

CHAPTER 3

3 EXPERIMENTAL SETUP AND WORK

3.1 Close Spaced Sublimation Technique

$Zn_{1-x}Cu_xSe$ thin films were deposited by Close Spaced Sublimation Technique, on glass substrate in vacuum chamber at room temperature. The schematic diagram of technique is shown in the Fig. 3.1.

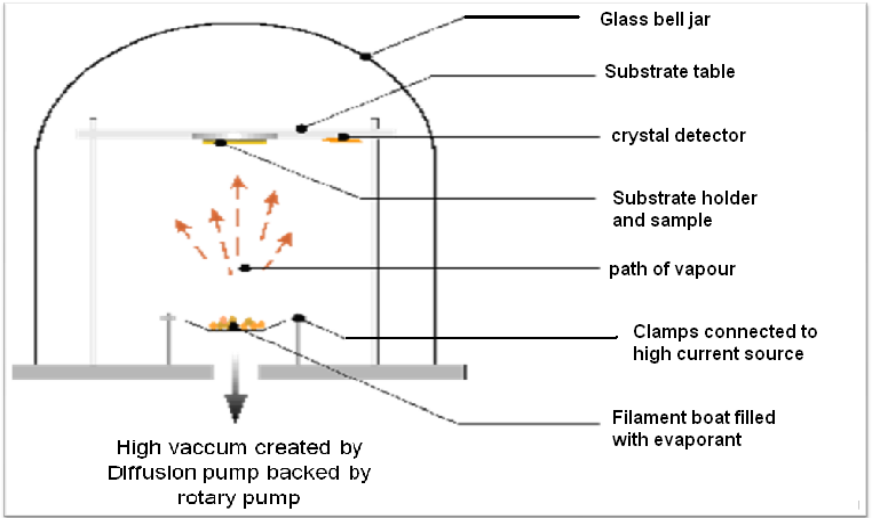

Fig. 3.1: Close spaced sublimation technique schematic diagram.

The main constituents of the experimental arrangement are given below

1. DC power supply
2. Vacuum chamber
3. Substrate holder
4. Optical films thickness monitoring by monochromatic light system.
5. Rotary and diffusion pumps for vacuum creation
6. Substrate heating system
7. Cooling system (chiller)
8. Resistive boats such as tungsten, molybdenum etc

The experimental set up is shown in Fig. 3.2

Fig. 3.2: Experimental set up of close spaced sublimation technique at NILOP

3.1.1 Solid Solution of $Zn_{1-x}Cu_xSe$

The $Zn_{1-x}Cu_xSe$ samples of 2 gram each have been prepared using the method of mechanical mixing for 1.5 hour each by pestle and mortar. Pure powder of ZnSe and Cu in molar concentration by using the following formula for each composition of material were prepared as

Mass of ZnSe = (X mol% × 2gm) ÷ total mol%

Mass of Cu = (X mol% × 2gm) ÷ total mol%

Where

X mol% = (molecular weight × X) ÷ 100

The molecular weight of ZnSe is taken as 144.33 and of Cu is 63.546. In the 2gm samples the concentration of Cu is increased by 5%, 10%, 15% and 20%.

3.1.2 Deposition of $Zn_{1-x}Cu_xSe$ thin films using close spaced sublimation technique

$Zn_{1-x}Cu_xSe$ thin films were deposited on glass substrates by close spaced sublimation technique at room temperature. A high vacuum coating unit (Edwards E-19/A) supported by a diffusion pump, has been used. Pressure inside the chamber was $\sim 2.6665 \times 10^{-3}$ Pa throughout the

deposition processes. High quality ZnSe and Cu, with ~99.999 purity, fine powder were taken in proper molar concentration and mixed for two hours to obtain a homogenous mixture with different concentrations of copper. In the 2 g samples the concentration of Cu (x) is increased to x = 0.05, 0.10, 0.15, 0.20. Homogenous mixture of $Zn_{1-x}Cu_xSe$ for various concentrations of Cu was heated by a halogen lamp (1000 W) connected to the main power through temperature controller with K-type thermocouple (Chromel & Alumel, 270 to 1350^oC). The evaporated powder was deposited on the rotating clean glass substrates at room temperature. The deposition time of all the samples is 5-7 minutes. The samples of all compositions were deposited under similar conditions. After deposition, the films were annealed at temperatures of 200^oC and 400^oC to observe the effect of the annealing temperature on the physical properties. In all cases the temperature increasing rate was about 5^oC/min.

Deposition parameters

Substrate temperature = Room temperature

Chamber pressure ≈ 10^{-5}mbar

Current = 30-40 Amperes

Deposition Time = 26-28 minutes

Deposition rate ≈ 0.2 nm/sec

3.2 Characterization Techniques Used for $Zn_{1-x}Cu_xSe$ Thin Films

1. Ion Beam Analysis (Rutherford backscattering spectroscopy)
2. Atomic Force Microscopy
3. Spectroscopic Ellipsometry
4. X-ray Diffraction

3.2.1 Ion Beam Analysis (IBA)

With the help of an accelerator facility, a family of analysis techniques generated by ion beam called IBA. IBA is composed of many analytical techniques which are purely a non-destructive process and based on interaction among the target material and fast moving energetic

ions. This ion-matter gives us concentration of the diverse elements present in matrix, elemental analysis, composition, thickness, depth profiling, location of impurities in single crystal, defect density and crystalline quality [1]. IBA includes following systems:

1. Rutherford Backscattering Spectrometry (RBS)
2. Particle (Proton) induces X-ray Emission (PIXE)
3. Ion channelling
4. Particle (Proton) Induced Gamma ray Emission (PIGE)
5. Elastic Recoil Detection Analysis (ERDA)

We concentrate and discuss only RBS technique.

3.2.1.1 Rutherford Backscattering Spectrometry (RBS)

RBS is a well described, non destructive, analytical, quantitative and unique fundamental investigational accelerator dependent tool [2]. For material examination, it is distinctive technique [3] broadly used in thin films for thickness, depth profiling of basic elements and elemental composition. Typically, for incident protons and He^{+} ions, analyzed depth is nearby 20 µm and 2 µm, respectively [2].

On a stationary target in RBS process a beam of He^{+2} (alpha particles) or H^{+} (protons) having energy generally 4 MeV to 0.5 is incident and to collect backscattered ions there is an energy sensitive detector by which we analyzed backscattered ions energy. Energies are depended on the features of target atom, depth into target sample up to which particles penetrate and scattering angle before scattering. Hence, RBS can be used for elemental analysis [6]. For first time in 1957 by Rubin et al. RBS was described as an experimental apparatus for material analysis and has since developed into main materials characterization method [2, 7].

RBS is a fast quantitative technique which does not need any reference standards, non-destructive and multi elemental analysis technique for the elements (Beryllium "Be" to Uranium "U") [3]. Typically high accuracy up to ±3% and have a depth up to ~2 - 10 nm [11]. Detection limit is about ~ 10^{18} cm^{-3} but RBS sensitivity in case of heavier elements is almost 100 ppm so it is not good for revealing lighter elements [4, 11]. Size of the beam spot varies from 0.5 - 2.0 mm [3]. The schematic diagram of RBS as experimental setup is shown in Fig. 3.3.

3.2.1.2 Instrumentation

RBS process can be done experimentally with help of ion beam analysis (IBA) device, which consist of three compulsory components, (i) ion source, (ii) linear particle accelerator and (iii) a particle detector [3]. The assemblage of these components is shown in Fig. 3.3.

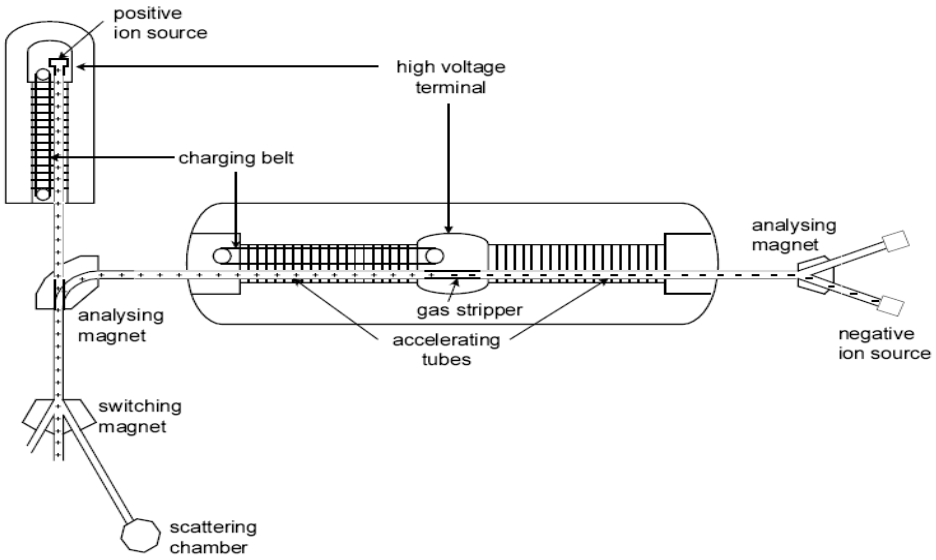

Fig. 3.3: Schematic of RBS instrument [8]

1. **Ion Source:** From ion source first a specific ion beam typically consisting protons or alpha particles are produced [7].
2. **Linear particle accelerator:** This ion beam is then accelerated towards target having energy usually in range of 0.5 to 4 MeV by choosing definite charge and mass for RBS operation. Electrostatic accelerator (Tandem Van de Graaff) is used for this purpose [7]. To acquire suitable beam for material inspection the accelerated beam is then conceded through scattering chamber which consists of switching and analyzing magnets. Now, this selected beam is presented to ultra-high vacuum and by means of magnetic or electrostatic lenses is positioned to the targeted material. Generally scattering takes place when ions collide with target sample [4, 7].
3. **Particle detector:** Solid state detector (silicon barrier detector) then collect ions scattered from target. Thus, along with compulsory electronics detector identifies corresponding

energy spreading of backscattered ions, which is finally examined and calculated by suitable computer program [7].

3.2.1.3 RBS Experimental Setup for the Characterization of $Zn_{1-x}Cu_xSe$ Thin Films

RBS analysis was performed **"using 5UDH-2 Pelletron Tandem Accelerator facility at National Centre for Physics (NCP), Experimental Physics Lab, Islamabad"** as shown in Fig. 3.4. The samples were illumined by well collimated beam of He^+ 2mm diameter and energy of 2.023 MeV. The sample was fixed in a vacuum chamber on a five-axis adaptable goniometer with an accuracy of 0.01°. The backscattering ions were logged by a surface barrier detector at a backscattering angle of 170° and energy resolution is 25.8keV. A beam integral connect with the sample frame was used to make sure the tests are repeatable and comparable and accept charge on sample from beam (dose 15μc).

Fig. 3.4: A 5UDH-2 Pelletron Tandem Accelerator at NCP, Islamabad.

3.2.2 X-Ray Diffraction (XRD)

X-Ray Diffraction is employed to study the crystal structure of bulk and thin solid films, including lattice constants, orientation of crystals, and preferred orientation of poly-crystals, surface and inner defects, grain size, strain, stress etc. It is a nondestructive technique and do not require complicated sample preparation or conducting film at the substrate.

Interference of the diffracted waves from different planes of atoms takes place generating a diffraction pattern. These diffraction patterns yield sharp interference peaks where the atoms are arranged in a periodic fashion. Brgag's law is used to find the condition for a diffraction peak to occur.

$$2d \sin\theta = n\lambda$$

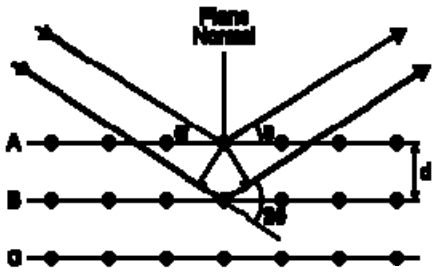

Fig. 3.5: Bragg's diffraction

Here, d is the inter-planar distance, θ is the scattering angle, n represents the order of the diffraction peak, and λ is the wavelength of the x-ray radiation as shown in Fig. 3.5. The snap of the XRD apparatus is shown in Fig. 3.6.

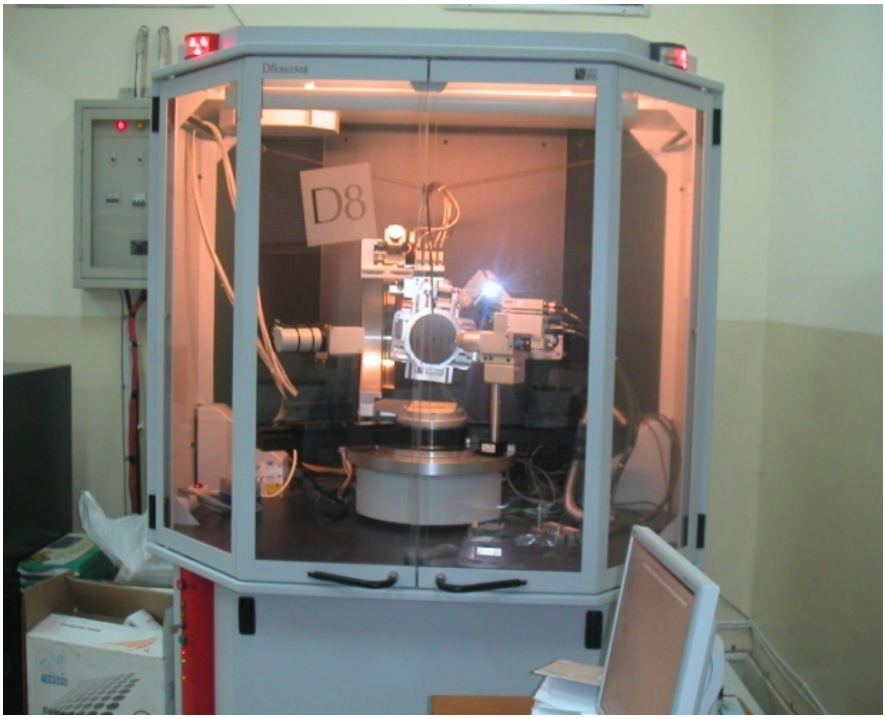

Fig. 3.6: (XRD) X-ray diffraction machine

A significant appliance of XRD is to attain an approximate of the crystallite size. This is very helpful as many material properties depend significantly on crystallite size [40, 41]. The crystallite size 't' or grain size may be calculated by means of Debye-Scherer formula:

$$t = \frac{K \times \lambda}{B \times \cos\theta_B}$$

Where K is a constant dependent on crystallite shape (0.9), λ is the wavelength of X-rays, B is full width at half maximum (FWHM), θ_B is the Bragg angle. According to the Scherer formula, the particle or grain size is inversely proportional to the width of a peak. There are different reasons of peak broadening e.g. strees/strain developed in the films or the instrument used.

3.2.3 Atomic Force Microscopy (AFM)

AFM measure the forces between a sharp probe/tip and surface at very short distance (0.2-10 nm probe-sample separation) and generate a 2 - 3D nanoscale profilometry of the surface. The probe is held on a bendable cantilever. The AFM tip softly touches the sample surface and records the force between the tip and the sample surface as shown in Fig. 3.7a.

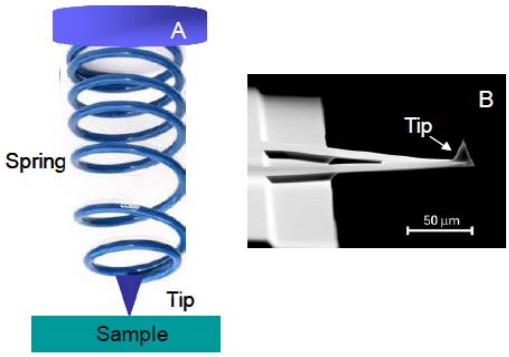

Fig. 3.7: (a) Spring illustration of cantilever (b) SEM image of cantilever with tip

The probe is positioned on the end of a cantilever. The quantity of force between the probe and surface depends on the stiffness (spring constant) of the cantilever and the distance among the tip and the surface. This force can be explained using Hooke's Law:

$$\mathbf{F = - k.x}$$

Where F is the Force, k is the spring constant and x is the cantilever deflection. AFM

cantilever typically has a spring constant of ~ 0.1 - 1 N/m. If this value is less than the stiffness of the surface, the cantilever bends and the deflection is observed. Tips are in general made from Si or Si_3N_4. Cantilevers of variable lengths and structural shapes allow for different spring constants and resonant frequencies. The movement of the tips across the surface is controlled by means of feedback and piezoelectric scanners. This scanner controls the bending of cantilever during the scanning over the sample. The deflections of cantilever are measured by a computer based programming to generate an image of the surface topography.

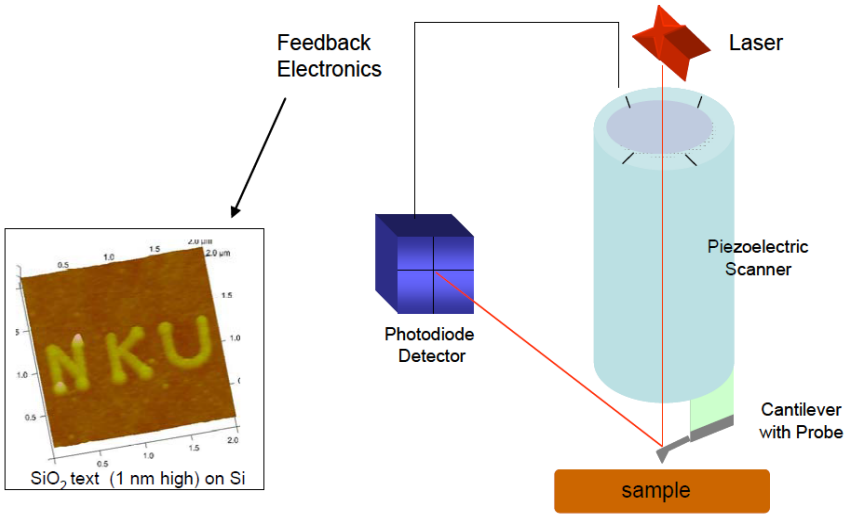

Fig. 3.8: AFM functioning schematic

3.2.3.1 Imaging Modes in AFM

The 3 primary imaging modes of AFM are:

(1) Contact mode
Tip and surface separation is less than 0.5 nm.

(2) Intermittent contact
Tapping mode, tip and surface separation is 0.5 - 2 nm.

(3) Non-contact mode
Tip and surface separation is 0.1-10 nm.

3.2.3.2 Applications of AFM

AFM is an incredible apparatus for imaging and determining nanometer size features. It has numerous characteristics that make it unique. Most of the measuring instruments need bigger sizes when better sensitivity is requisite but AFM has the ability of built-in atomic-scale

sensitivity. Hence there is no need to make AFM instrument larger for more sensitive. AFM is also used for fabrication technology and creating changes in surface structures at the nanometer extent. A very accurate control on the motion of the tip is always required to precisely scan the surface at the nanometer scale. AFM permits such accurate movement and control technology which is also cost effective than other methods.

Surface morphology of the $Zn_{1-x}Cu_xSe$ was imaged by Quesant Universal SPM Atomic force microscopy (QScope™ 350) in non contact method. An AFM tip of Si_3N_4 having a radius of curvature of 10 nm was used. Both topography and phase (2 - 3 D) images were measured at the same time. All the images were recorded in scanning areas of 2 - 5 μm^2 at scan rate of 1.0 Hz and 600 x 600 pixels resolution. Collected images were analyzed by using Nova Px software (NT-MDT Co.) thus generating RMS surface roughness.

3.2.4 Spectroscopic Ellipsometery (SE)

Ellipsometry is utilized to characterize thin films microstructure, optical and dielectric constants and surface roughness. SE is very perceptive measurement method that uses polarized light. Reflected polarized light change its relative phase in a beam which drives its sensitivity, beyond the sensitivity of intensity reflectance measurement. SE is a non contact and non destructive method. No vacuum is obligation compared with all ion-beam or e-beam based instruments. No need of standards or reference because ellipsometry is an absolute method. It provides twice more information (both amplitude and phase ratio) than reflectometry (only intensity). In addition, as ellipsometer does not deals with the intensity but with polarization state so it is less sensitive to fluctuations in light intensity. For thin film characterization therefore it is the best non-destructive technique. Both imaginary and real part of the complex refractive index dielectric function can be obtained. With great accuracy film thickness can be calculated.

3.2.4.1 Ellipsometer Measurements

Through the surface of sample, ellipsometry determine the change in polarization state of light transmitted from or reflected. Basically, ellipsometry refer only to extent of polarization state of light beam. However, polarization state of a beam of light modifies by optical system are usually measure by the ellipsometert. Optical system is simply the sample, for thin film analysis.

The calculated values are articulated as delta (Δ) and psi (ψ). These values are associated to the ratio of R_p and R_s (Fresnel reflection coefficients) for correspondingly p and s polarized light.

$$\rho = \frac{R_p}{R_s} = \tan(\psi)e^{i\Delta}$$

Ellipsometery is very reproducible and highly accurate because it calculates the ratio of two values. This ratio also contain phase information and is complex number that's why the measurement very perceptive.

3.2.4.2 Parameters Determined by Ellipsometer

To characterize both bulk materials and thin films ellipsometry is usually used. Thin film optical constants and the thickness are most common applications of this measurement. It also is the major technique for finding optical parameters in IR, Visible and UV wavelength ranges. To many material properties ellipsometry is very sensitive and flexible. Very diverse parameters such as reflection, transmission, absorption, optical constants, doping concentration, thin film thickness and crystallinity etc. can also be measured by ellipsometry.

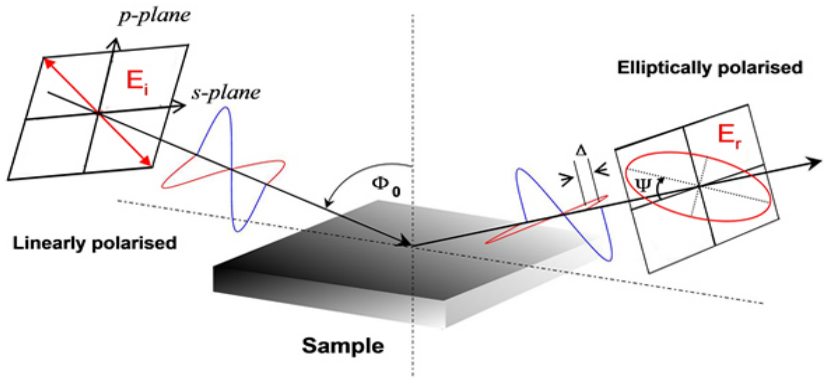

Fig. 3.9: Schematic diagram of spectroscopic ellipsometry technique

The schematic diagram for ellipsometry is shown Fig. 3.9. The light is first prepared monochromatic, collimated, and then linearly polarized. Upon transient by the compensator (generally a quarter-wave plate), circularly polarized is obtained and then specimen surface is illuminated. The light is transmitting through a following polarizer after reflection, which serves

as the analyzer. Lastly, the light intensity is calculated quantitatively by a detector (photomultiplier) or judged by eye. Until light extinction occurs the analyzer and polarizer are rotated. The amplitude ratio of the two components of reflected light determined and extinction readings enable to check the phase difference. From these, either the index of refraction or the thickness of film can be obtained. The schematic of the ellipsometry arrangement is shown in Fig. 3.10.

Fig. 3.10: Spectroscopic ellipsometry system at NILOP

3.2.4.3 Methods in Ellipsometry for Data Analysis

Obtain Ψ and Δ (phase and amplitude changes) data versus angle of incidence and wavelength. Formulate an optical model that describe as much as possible the information about sample structure. All layers in the sample structure must be counted. Create (simulate) an optical model by which theoretical data obtained must match to the data obtained experimentally and compare them. Unknown parameters such as optical constants or thin film thickness or both in the optical model are varied until "best fit" to experimental data. To vary unknown parameters regression algorithms are used and diminish the difference between the experimental and generated data. Once a good "fit" to the experimental data is achieved, sample's physical parameters such as optical constants, film thickness, surface roughness, composition etc are obtained. The dielectric constant, film thickness and band gap energy (Eg) of the deposited films were measured by a spectroscopic ellipsometer (J.A. Woolam M-200VI). At an incidence angle of 70^{o} the experimental delta (Δ) and psi (Ψ) spectra were recorded.

3.3 References

1. W. D. Nix and B. M. Clemens. Crystallite coalescence: A mechanism for intrinsic tensile stresses in thin films. J. Mat. Res. **14** (1999) 3467-3473.
2. M. Mayer. Rutherford Backscattering Spectrometry (RBS). Lectures given the workshop on Nuclear Data for Science and Technology: Material Analysis Trieste (2003).
3. H. R. Verma. Atomic and Nuclear Analytical Methods. Springer Berlin Heidelberg New York (2007). ISBN-10 3-540-30277-8.
4. K. C. Singh. Basic Physics. ISBN-978-81-203-3708-4.
5. The Rutherford scattering experiment. (2004). www.physik.unibas.ch/Praktikum/VpII/PDF/Rutherford.pdf
6. Sven A. E. Johansson, John L. Campbell, Klas G. Malmqvist. Particle-Induced X-Ray Emission Spectrometry (PIXE) (1995)
7. F. Corni, G. Ottaviani, M. Michelini, G. L. Michelutti, L. Santi, A. Stefanel. Rutherford Backscattering Spectrometry: A technique worth introducing into pedagogy. GIREP (1995).
8. Instrumentation for PIXE and RBS. IAEA, VIENNA (2000) www.pub.iaea.org/MTCD/publications/PDF/te_1190_prn.pdf.
9. B. D. Cameron, M. J. Rakovic, M. Mehrubeoglu. Measurement and calculation of the two-dimensional backscattering Mueller matrix of turbid medium. Optical Letters 23 (1998) 485-487.
10. Khalid Hossain. A Novel Process for Germanium Silicide Thin Film Synthesis. University of North Texas (2007).
11. http://mse.hanyang.ac.kr/SNE/.pdf.
12. G. Shmalz, V. Deutscher, U. Glatte and Ebenheit als physikalisches und physiologishes Problem. (1929) 1461-1467.
13. Apparatus for measuring surface irregularities. U.S. Patent 2,728,222.
14. Tunnel liner bolt tightening apparatus. UK Patent 2,009,409.
15. R. Young, J. Ward, F. Scire, The Topografiner: An Instrument for Measuring Surface Microtopography. Rev. Sci. Inst. **43** (1972) 999.

16. G. Binnig, H. Rohrer, Ch. Gerber, E. Weibel. Surface Studies by Scanning Tunneling Microscopy. Phys. Rev. Lett. **49** (1982) 57.
17. G. Binnig, C. F. Quate, Ch. Geber. Atomic Force Microscope. Phys. Rev. Letters **56** (1986) 930.
18. Y. Martin, C. C. Williams, H. K. Wickramasinghe. Atomic Force Microscope-Force Mapping and Profiling on a sub 100-E scale. J. Appl. Phys. **61** (1987) 4723.

CHAPTER 4

4 RESULTS AND DISCUSSION

The results of the compositional, structural and optical analysis of the deposited samples by RBS, XRD, AFM and spectroscopic ellipsometry are discussed in this chapter. The films were obtained throughout the composition range ($0 \leq x \leq 0.20$). The structural properties were analyzed by X-ray diffraction with Cu, Kα radiation. Spectroscopic Ellipsometry (SE) has been employed to determine the band gap energy and dielectric constant ε_1 of the films.

4.1 Rutherford backscattering (RBS)

The RBS experiments were made on $Zn_{1-x}Cu_xSe$ thin films of varying compositions deposited on glass substrates. A detailed study was carried out for both the as grown and annealed films of various thicknesses. The gathered RBS spectra were then fitted by the code RUMP [1] to locate the comparative concentrations of a mixture of elements in the films. Fig.4.1 (a-b) shows the RBS spectra of as-grown and annealed films of $Zn_{1-x}Cu_xSe$ (x= 0.10, 0.15) which proves that the simulated spectra of the deposited films are in good agreement with the measured data.

The energy spectrum of the emitted ion yields information about the concentration depth profiles. The composition has been altered and copper was seemingly introduced into the layers as a substitutional metallic participant as seen through RBS spectra. The composition of the samples was calculated and compared with the original percentage which shows that composition is nearly stoichiometric and the accurate incorporation of added copper is observed. The spectra shows that the deposited films mainly have a Zn(Cu)xSe chemical composition, with x varying from $0.10 \leq x \leq 0.20$ at the surface area and then declining with depth. Maximum concentration of the doped Cu is present at the surface (~100-200 nm) layers. It consists of three superimposed elemental yields of three species at different channels. Moreover, it can be seen that there is no impurities or contamination in the as-deposited films while small percentage of oxygen and silicon is seen in the spectra which are coming from the substrate signal.

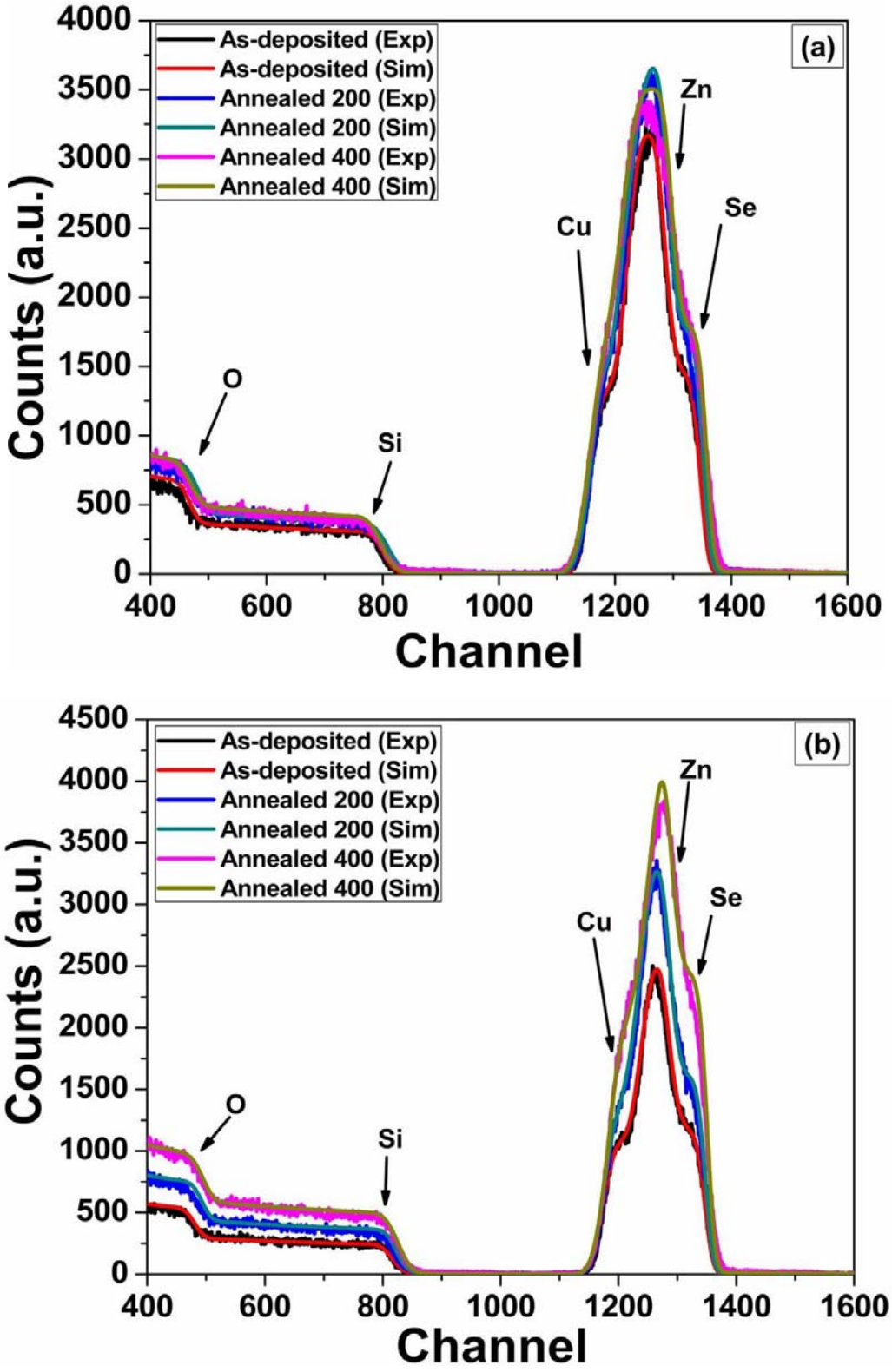

Fig. 4.1: Rutherford backscattering spectra of as-deposited and annealed (200ºC and 400ºC) $Zn_{1-x}Cu_xSe$ (a) x=0.10, (b) x=0.15.

The peaks of the heavy elements (Zn, Se and Cu) can noticeably be separated by the He^+ beam and accordingly can be used to resolve the comparative thickness and stoichiometry of the films. The uppermost channel number corresponds to the highest backscattered He^+ ions energy from the element Se present in the film sample. The edge arising at a channel just below 950 is due to the silicon present in the substrate. The energy channel correspondence to zinc is 1285; zelenide is 1344 while for copper is 1152.

After annealing, as the RBS spectra turns into slightly broader and sharper so there could be a prospect of channeling. Annealing play an important part in altering the film thickness and prominent change in elemental ratio with respect to stoichiometry within the layers has been observed as shown in table 4.1. As the progress in semiconductor thin film technology is advancing, the thickness of device circuits is becoming very thinner and thinner. Therefore, an accurate measurement for film thickness is required. For thin targets, the scattering is proportional to the target thickness. Angular frequency changes as the mass of the constituent's changes within the sample from which we can estimate the thickness accurately by using RBS. The broadness observed in the RBS peaks indicates the increase in thickness of the films [2].

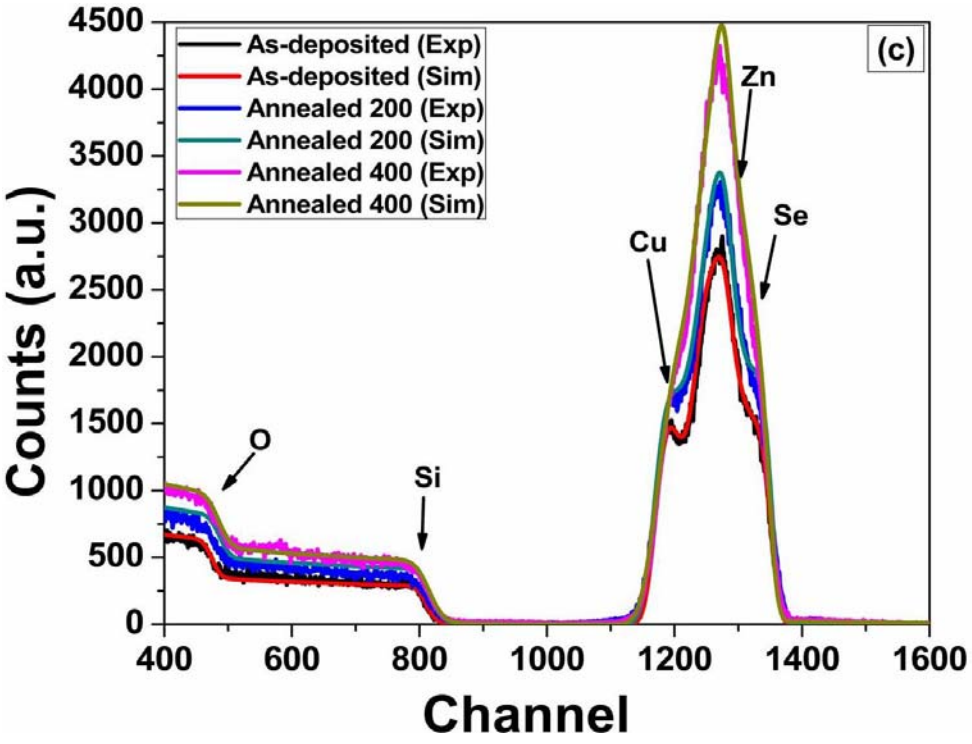

Fig. 4.2: Rutherford backscattering spectra of $Zn_{1-x}Cu_xSe$ (x=0.20) films

It was noticed that a protuberant edge occurs at ~1152 elemental yield for copper content which is only prominent for x=0.20 as shown in Fig. 4.2. This edge arises due to the excessive enrichment of Cu in the ZnSe matrix and corresponds to the unbound Cu content which subsists on the surface. By increasing annealing temperature this edge shows declination and fades at 400°C annealed temperature. From this it is certain that diffusion of copper into ZnSe matrix increases with increasing annealing temperature. According to the RUMP simulation software, 400°C annealed films exhibit the most homogeneous Cu concentration as a function of depth as compared to other studied samples. Thickness of the films estimated by RBS technique, spectroscopic ellipsometery and quartz crystal are in good agreement. Moreover, the deposited films were homogeneous, even and well adherent with the substrate. The analyzed compositions and thicknesses of the composite films are shown in table 4.1.

Table 4.1

Film thickness and compositional analysis investigated by spectroscopic ellipsometer (SE) and Rutherford backscattering spectroscopy (RBS) of $Zn_{1-x}Cu_xSe$ thin films for various Cu concentrations (X).

Film Composition	Nature	Film thickness		Composition by RBS		
		Spectroscopic ellipsometer	RBS	Zn	Se	Cu
X=0	As-deposited	255.1	240	0.5	0.5	0
	Annealed 200	239.42	230	0.5	0.5	0
	Annealed 400	222.17	220	0.5	0.5	0
X=0.05	As-deposited	297.48	290	0.450	0.500	0.050
	Annealed 200	310.96	300	0.470	0.480	0.050
	Annealed 400	315.62	300	0.470	0.480	0.050

Film Composition	Nature	Film thickness		Composition by RBS		
		Spectroscopic ellipsometer	RBS	Zn	Se	Cu
X=0.10	As-deposited	219.56	210	0.480	0.420	0.100
	Annealed 200	230.62	215	0.480	0.420	0.100
	Annealed 400	250.7	255	0.450	0.450	0.100
X=0.15	As-deposited	189.38	180	0.420	0.430	0.150
	Annealed 200	197.09	185	0.450	0.400	0.150
	Annealed 400	201.01	190	0.400	0.450	0.150
X=0.20	As-deposited	210.63	195	0.320	0.480	0.200
	Annealed 200	211.78	200	0.330	0.470	0.200
	Annealed 400	222.64	210	0.380	0..420	0.200

4.2 Structural characterization

4.2.1 X-ray Diffraction (XRD)

To investigate the crystal structure, composition and phase, as-deposited and annealed $Zn_{1-x}Cu_xSe$ thin films were investigated by using X-ray diffraction (XRD) machine. The X-ray diffraction pattern of $Zn_{1-x}Cu_xSe$ thin films are shown in Fig. 4.3 and Fig. 4.4**.** ZnSe thin film is confirmed as a zinc-blende structure with preferential orientation along the (111) plane [3]. In the present work, the XRD pattern of as-deposited samples exhibit more than one peak. Fig. 4.3 shows the XRD graph of $Zn_{1-x}Cu_xSe$ films annealed at 400ºC with two different copper concentrations (X= 0, 0.15) while Fig. 4.4 shows XRD pattern of as-deposited and annealed (200ºC and 400ºC) $Zn_{1-x}Cu_xSe$ thin films for 5% and 15% Cu concentration. Doping of Cu into ZnSe do not have effect on the crystal structure until 10% of Cu and consequently no secondary phase has appeared for Cu. Actually, Zn^{2+} (74 pm) has close ionic radius with Cu^{2+} (73 pm), as a

result Cu can easily penetrate into ZnSe to replace Zn positions in the crystal lattice without making any change in the basic crystal structure and forming a mono phase [4-6]. XRD patterns indicate that the increase of annealing temperature leads to improvement of the ZnSe films growth on the favored (111) orientation, This is due to the decrease in film stresses and grain coarsening as confirmed by the RBS results. Small crystallites can fuse together to make larger crystallites, resulting in micro cracks and surface roughness [7]. Annealing is well-known in reducing the stress of film as well as decreases the d-spacing. After annealing, the intensity of (220) and (311) reflection decreases while the preferred orientation in (111) direction increases radically at 400°C and this strongly preferred orientation may reduce the contact area between grains.

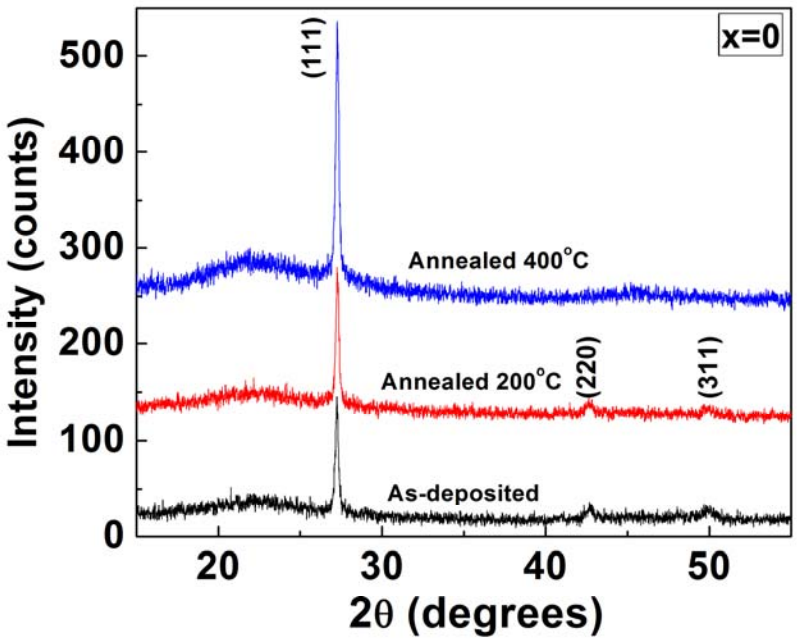

Fig. 4.3: XRD pattern of as-deposited and annealed (200°C and 400°C) $Zn_{1-x}Cu_xSe$ thin films

It is evident that the replacement of Zn with Cu atoms in the lattice sites in the host material causes the Zn to shift to another lattice point within the crystal resulting in the enhancement of crystallite size and the crystallinity. Nevertheless, the crystalline quality drops when Cu doping concentration is increased beyond 10%. During deposition, the grains in the 15% and 20% Cu doped ZnSe films grow along the (102) direction which shows that the grains

are reoriented and a new plane (102) has appeared which has maximum intensity at 20%. The peak corresponding to (102) direction indicates that the prepared films at this concentration are polycrystalline in nature with wurtzite phase. Because the synthesis process is affected by the introduction of impurity Cu ions into the host lattice of ZnSe which can significantly affect the deposited films causing a reduction in the crystal phase [8].

Fig. 4.5 shows the effect of annealing on the FWHM for (111) orientation. This can be increased or decreased depending on coalescence and recrystalization of grains. Recrystalization may help (111) orientation and peak growth, making the FHWM smaller. It is observed that with the increase in annealing temperature the value of FWHM decreases. This decrease in FWHM may be due to grain growth and crystallinity enhancement. Improvement in crystallinity may be attributed to a decrease in defect density with annealing. The initial decrease in FWHM up to 10% Cu concentration as can be noticed in Table 4.2, this could be related with improvement of crystallinity because of desorption of oxygen. When annealing at temperature of 200°C, slight modification of the crystal structure is observed, however the crystal structure changes significantly after annealing at 400°C. A slight decrease in diffracting angle 2θ for x= 0.15 annealed at 400°C is also observed which confirms that after annealing the grains are re-crystallized and coalescence is assumed to happen.

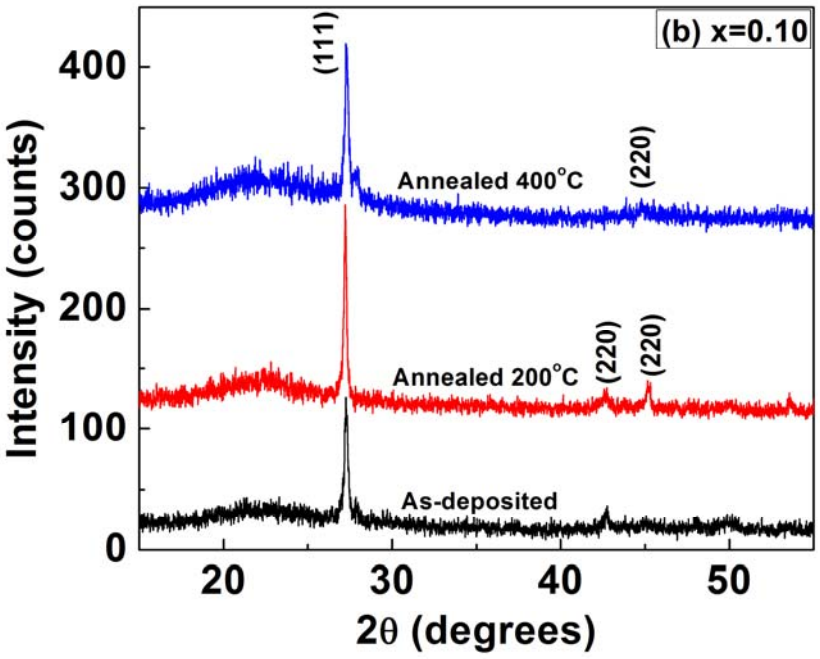

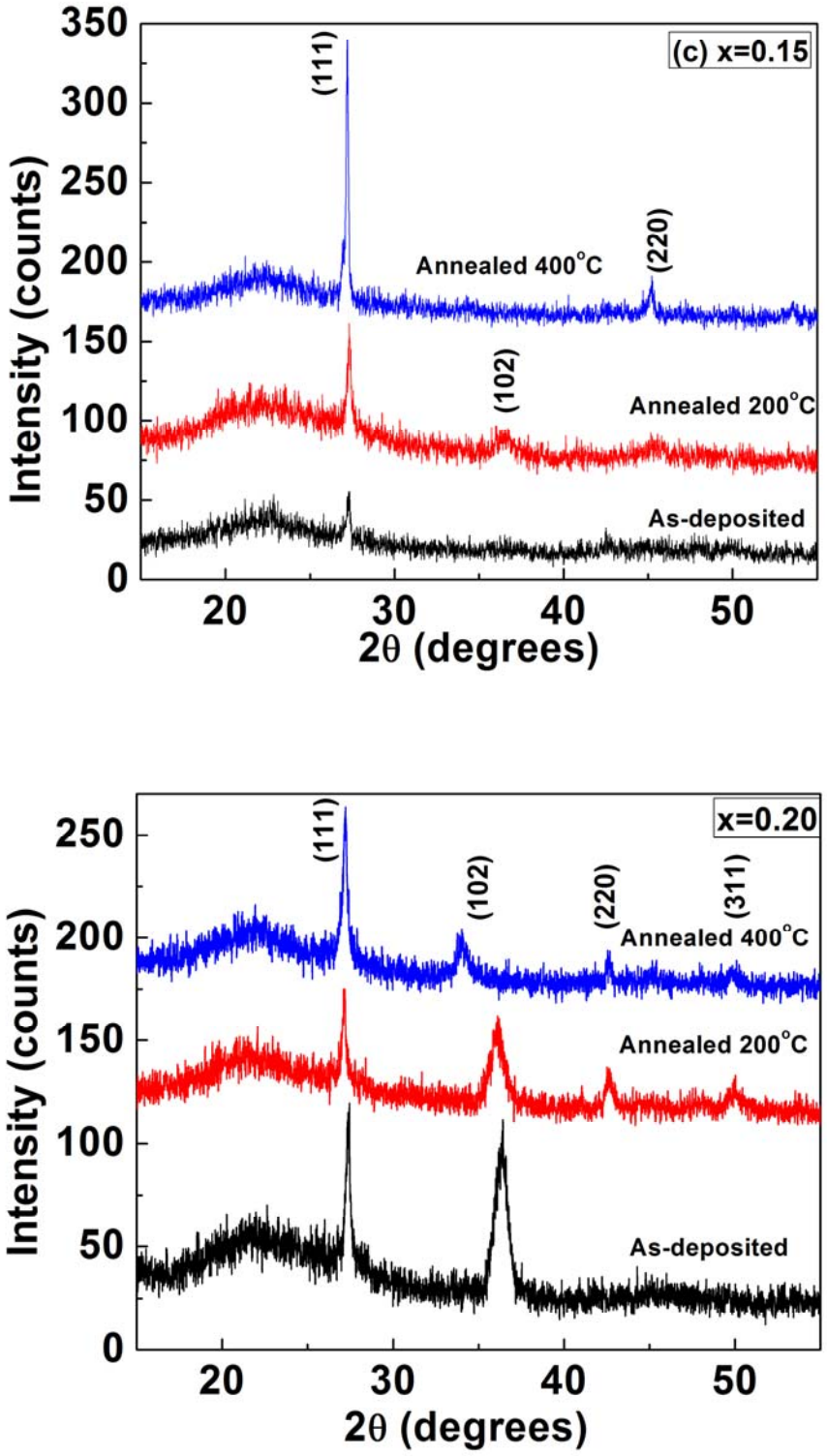

Fig. 4.4: XRD pattern of as-deposited and annealed (200ºC and 400ºC) $Zn_{1-x}Cu_xSe$ (x= 0.10, 0.15, 0.20) thin films

The stacking fault energy (SFE) for the as-deposited and annealed films is calculated for (111) plane by using the relation.

$$SF = \left[\frac{2\pi^2}{45\left(3\tan\theta\right)^{1/2}} \right] \beta \qquad (1)$$

Where 'β' is the full width at half maxima (FWHM) and 'θ' is the Bragg's angle. The stacking fault energies were estimated from the reallocation of the peaks of the X-ray lines with reference to JCPDS database No: 89-7130 (2003), using eq. (1). Fig. 4.5 shows that stacking fault energy decreases gradually with increasing copper concentration up to 10 % and crystal growth becomes sharp while an opposite trend is monitored beyond this Cu concentration. SFE also decreases with increasing annealing temperature. It can be seen that SFE for 0% Cu concentration decreases from 0.07335 to 0.04431 for as-deposited and 400ºC annealed films, while for 20% Cu concentration it decreases from 0.08277 to 0.05972. All the structural parameters are summed up in table 4.2.

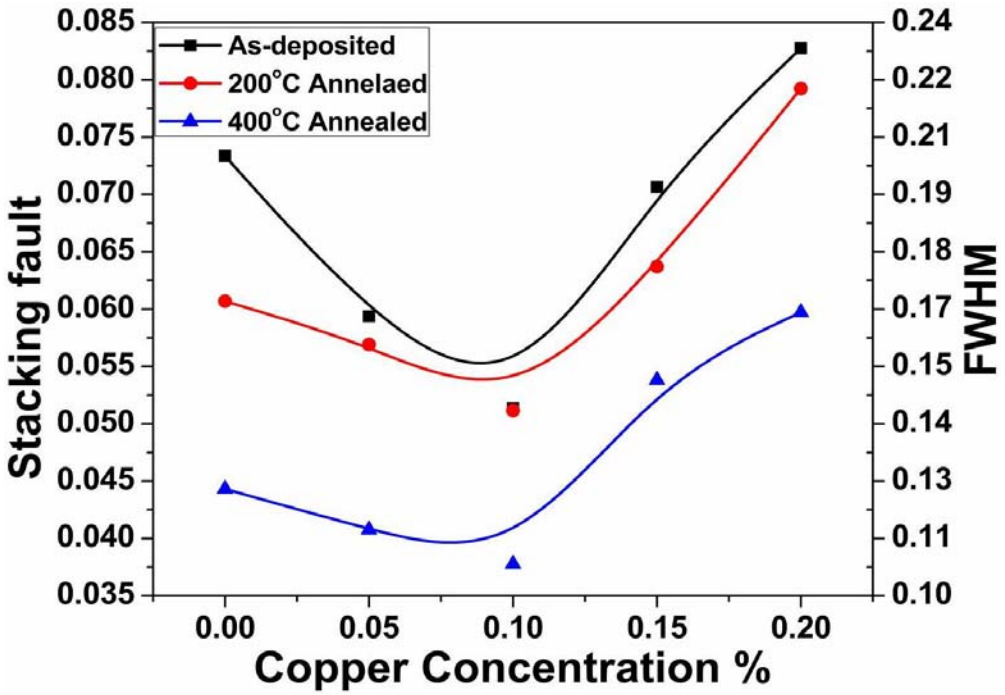

Fig. 4.5: Variations of Full width half maxima (FWHM) and Stacking fault energy of as-deposited and annealed (200ºC and 400ºC) $Zn_{1-x}Cu_xSe$ thin films with Cu concentration

Table 4.2

Peak position (2θ), full width half maxima (FHHM), stacking fault, Band gap and mean square roughness (RMS) of as-deposited and annealed (200ºC and 400ºC) $Zn_{1-x}Cu_xSe$ thin films for various Cu concentrations (X).

Film Composition	Nature of films	2θ in degree [37]	FWHM (2θ)	Stacking fault	Band gap (eV)	Roughness (nm)	
						AFM	Spectroscopic ellipsometry
X=0	As-deposited	27.28	0.1968	0.07335	2.74	1.11	12.18
	Annealed 200	27.23	0.1581	0.06068	2.76	9.29	16.51
	Annealed 400	27.24	0.1168	0.04431	2.78	-	16.41
X=0.05	As-deposited	27.26	0.1574	0.05937	2.70	1.25	7.99
	Annealed 200	27.22	0.1474	0.05691	2.74	-	27.67
	Annealed 400	27.25	0.1074	0.04075	2.77	-	15.61
X=0.10	As-deposited	27.28	0.1378	0.05136	2.68	1.39	19.77
	Annealed 200	27.27	0.1364	0.05114	2.73	-	15.61
	Annealed 400	27.22	0.0978	0.03776	2.75	-	11.31
X=0.15	As-deposited	27.35	0.1978	0.07064	2.62	1.21	33.34
	Annealed 200	27.33	0.1762	0.06371	2.63	-	40.67
	Annealed 400	27.2	0.1378	0.05381	2.67	-	14.09
X=0.20	As-deposited	27.38	0.2362	0.08277	2.61	1.08	6.53
	Annealed 200	27.14	0.1962	0.07923	2.62	-	30.69
	Annealed 400	27.25	0.1574	0.05972	2.65	-	19.20

4.2.2 Atomic Force Microscopy (AFM)

The surface morphology of the surface in 2D and 3D is shown for each image with its corresponding z-axis. The morphology of $Zn_{1-x}Cu_xSe$ films was examined through these AFM images. Fig. 4.6-4.8 shows the image obtained for the deposited films in an area of 2-5 μm^2. The

creation of a large number of closely bound particles of different sizes can be seen in these images. A roughness average (RMS) of the homogeneous films surface is being measured in this area which is listed in table 4.2. These formations are in agreement with those reported by Mazon-Montijo et al. [5].

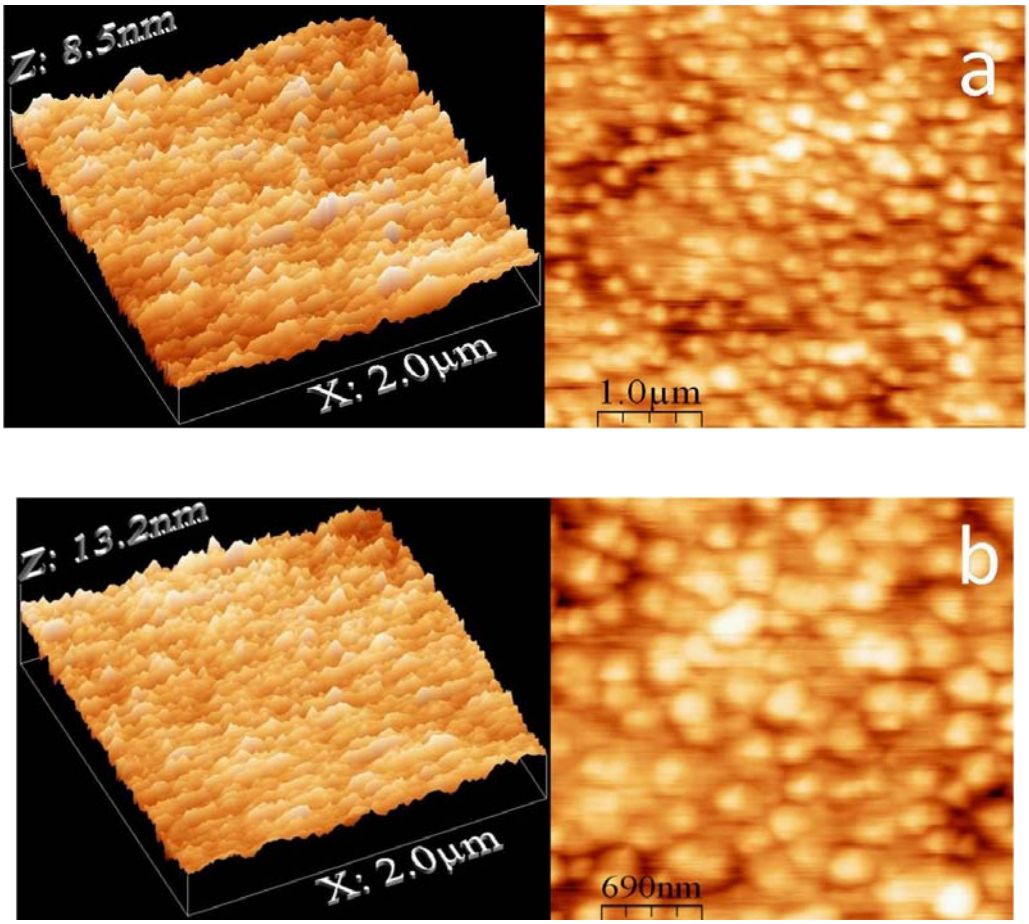

Fig. 4.6: AFM 2-D and 3-D images of as-deposited (a) x= 0.00 and (b) 0.10 thin films

Fig. 4.6 (a, b) indicates the surface morphology of as-deposited $Zn_{1-x}Cu_xSe$ (x=0.00, 0.10) films. These images present a low roughness with grain size of 8.5 nm for 0% Cu concentration (fig. 4.6a), over a scan size of 2 μm^2, which suggests the formation of very smooth surface. The grain size is observed to increase with Cu concentration as shown in fig. 4.6b. The increase in grain size is due to the increase in Cu concentration as well as the improved crystallinity as observed from the XRD results. It is observed that surface roughness (RMS)

increases from 1.12 nm to 1.39 nm for x = 0.00 to 0.10 as-deposited films respectively with increase of Cu concentration.

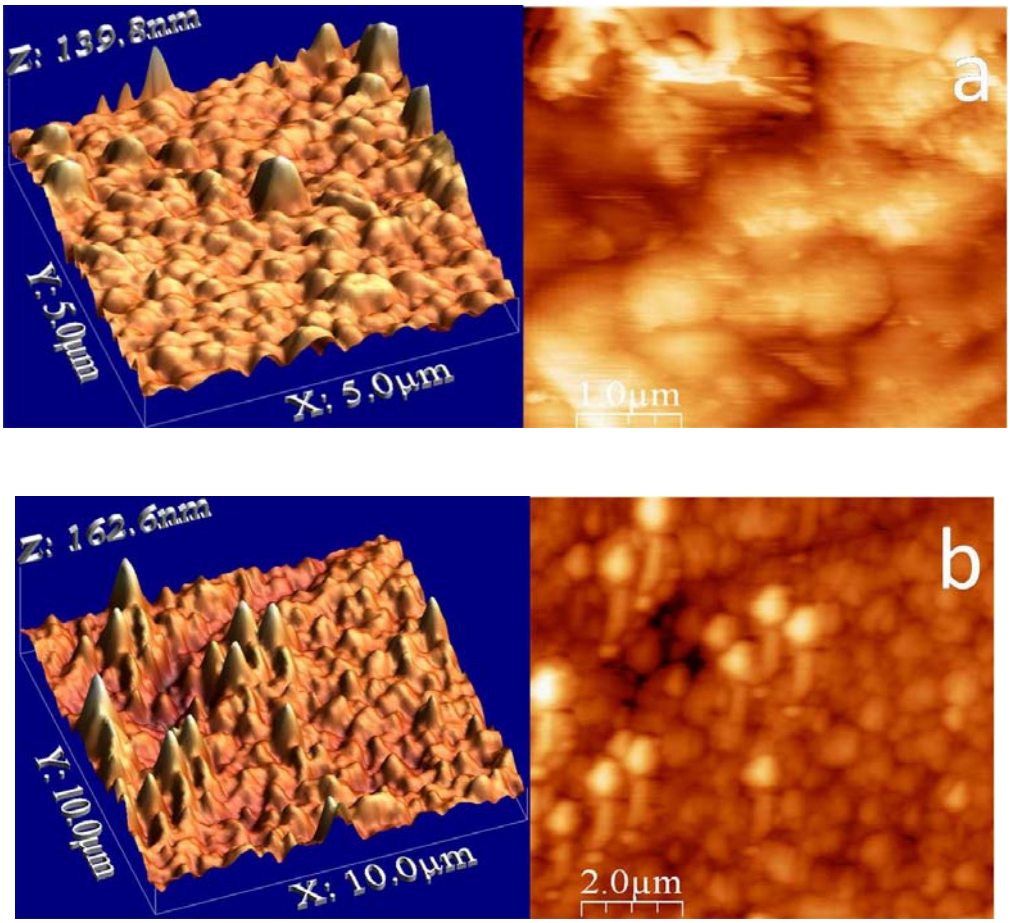

Fig. 4.7: AFM 2-D and 3-D images of 200°C annealed (a) x= 0.00 and (b) 0.10 thin films

Fig. 4.7 (a, b) shows the surface morphology of the 200°C annealed films. The islands shaped after heat treatment at 200°C shows that they are not uniform and clusters are shattered. 2-D images also indicate that there is proper cluster formation of the particles and the surface morphology is enhancing. The islands formed on the surface of the films annealed at 400°C shows the improvement in particle size along with improved micro-asperities besides these islands as shown in Fig. 4.8 (a, b). This image is very descriptive to view the existence of clusters on the surface and cluster-by-cluster mechanism is recovered after annealing at 400°C.

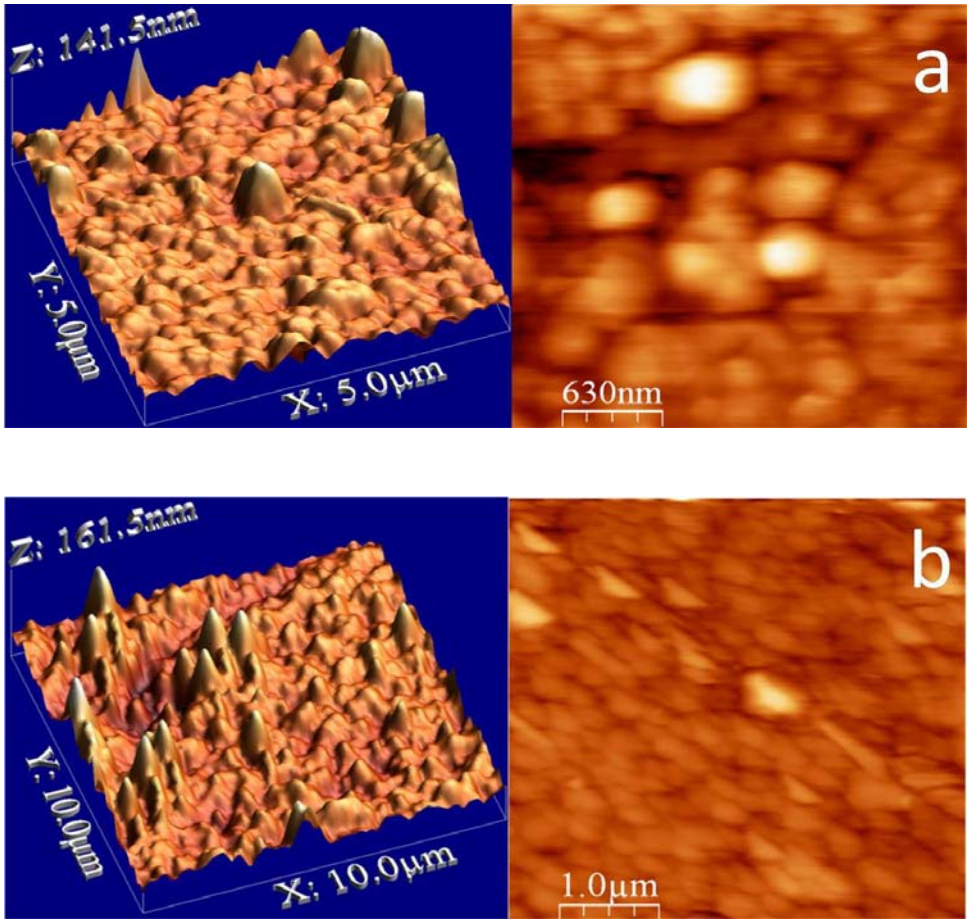

Fig. 4.8: AFM 2-D and 3-D images of 400°C annealed (a) x= 0.00 and (b) 0.10 thin films

Careful comparison between figs. 4.7 and 4.8 reveals that the micro features at the surroundings of islands after annealing at 400°C are almost similar in shape to 200°C annealed films but the size of the particles are reduced after 400°C annealing. This indicates that the larger grains are replaced by smaller and fine grains (micro-asperities) at 400°C accompanied by a decrease in RMS value from 1.55 nm to 1.11 nm. Accordingly, the grain size as calculated from XRD peak broadening was 41.64 nm after heat treatment at 400°C as compared to 32.20 nm in films annealed at 200°C.

4.3 Optical Characterization

4.3.1 Spectroscopic Ellipsometry

Spectroscopic ellipsometer has been employed to estimate the band gap (E_g) and dielectric constant (ε_1) of the deposited $Zn_{1-x}Cu_xSe$ thin films. A beam of polarized light is illuminated onto the sample and polarization change is précised by reflection data. The polarization change is detected by the ellipsometer and then simulated by ellipsometry psi (Ψ) and delta (Δ) parameters defined by the equation.

$$\tan(\psi).e^{i\Delta} = \rho = \frac{r_p}{r_s} \qquad (2)$$

Where, tan (Ψ) is the magnitude of the reflectivity relation, Δ is the change in phase, r_p is the p-polarized light reflectivity and r_s is the s-polarized light reflectivity. The experimental psi (ψ) and delta (Δ) spectra were record as a function of wavelength over the range: 400-800 nm at an incidence angle of 70°. These parameters are associated with thin film optical properties by the above equation [5]. A model was employed to fit the experimental data with theoretical data in order to find the film thickness and optical constants. For this effective medium approximation (EMA) model is used. Calculated and simulated psi (Ψ) and delta (Δ) spectra for as-deposited pure ZnSe thin film is plotted as shown in the Fig. 4.9.

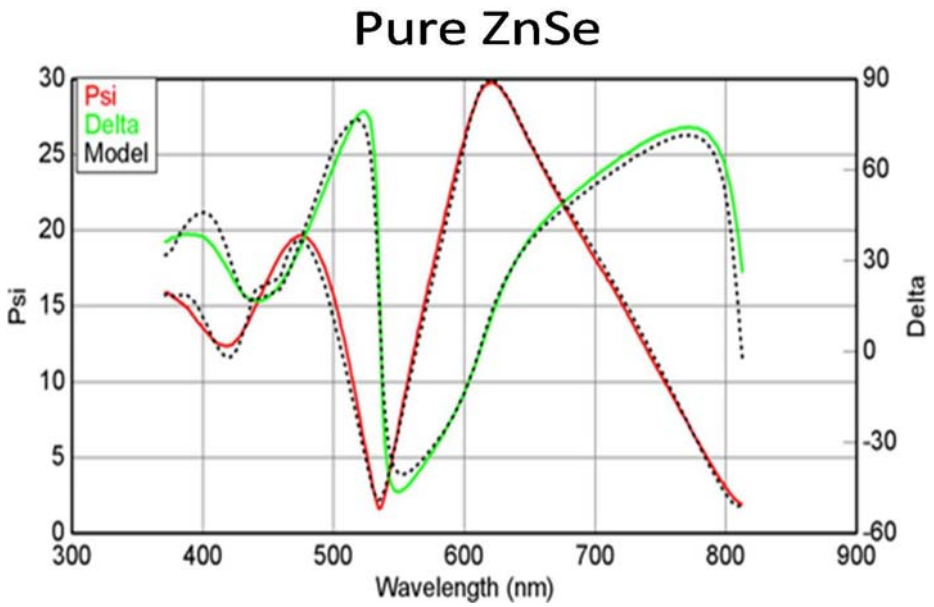

Fig. 4.9: Curve fitting of psi and delta by Ellipsometry

From the graph it is clear that the experimental values are well fitted with simulation. The fitting of the curve shows that the EMA model was exact. Using this curve fitting, film thickness and band gap was estimated. The band gap energy was determined using the Tauc's relation. Generally the Tauc's relation can be written as:

$$\alpha h\nu = A(E_g - h\nu)^m \tag{3}$$

Where α is the absorption coefficient and *k* is the extinction coefficient. Absorption co-efficient 'α' has been calculated using the relation.

$$\alpha = \frac{-\ln T}{t} nm^{-1} \tag{4}$$

Where T is the transmittance at a particular wavelength and t is the film thickness which is calculated by RBS. In eq. (3) 'm' is the half integral for allowed direct band transition. Therefore for m=1/2 the above equation can be written as

$$\alpha h\nu = A(E_g - h\nu)^{1/2} \tag{5}$$

$$(\alpha h\nu)^2 = A(E_g - h\nu) \tag{6}$$

The band gap energy is acquired by plotting a graph between $(\alpha h\nu)^2$ (on y-axis) and hν (on x-axis). The values of the band gap energy are predicted by extrapolating the linear portion of the curve to $(\alpha h\nu)^2 = 0$ for each sample. The linear nature of the plots at the absorption edge shows that $Zn_{1-x}Cu_xSe$ is a semiconductor with direct band gap. By putting $(\alpha h\nu)^2=0$ in the eq. (6), the R.H.S of the above eq. becomes

$$A(E_g - h\nu) = 0 \tag{7}$$

$$E_g = h\nu \tag{8}$$

$$E_g = hc/\lambda \tag{9}$$

It is recognized that the optical band gap of polycrystalline ZnSe semiconducting thin film is higher than that of bulk ZnSe ~ 2.6 eV due to quantum size effects as shown in Fig. 4.10 (a-c) [8]. Eg values of the as-deposited films increases from 2.74 to 2.78 eV as the annealing temperature increases from room temperature to 400°C as shown in Fig. 4.10a. The band gap of the 200°C and 400°C annealed ZnSe (x=0) thin films were found to be 2.76 eV and 2.78 eV, which shows 0.06 eV red shift for 200°C annealed and 0.08 eV red shift for 400°C annealed film from the normal bulk value (2.70 eV). The increase in band gap from 2.74 eV to 2.76 eV and 2.78 eV shows that annealing the film causes strong red shifts of 0.02 eV and 0.08 eV in the optical spectra to that of as-deposited ZnSe films. Moreover, the band gap of Cu doped films show similar results as that of pure ZnSe films. Table 4.2 shows that band gap energy decreases as the Cu concentration increases in the ZnSe matrix. The variation of band gap energy with annealing temperature is found to be almost linear as shown in the inset of fig. 4.10 c. Our calculated values of optical band gap by spectroscopic ellipsometer are slightly greater than reported by J. Kvietkova et al and Dahmani et al by using spectroscopic ellipsometer [9-10].

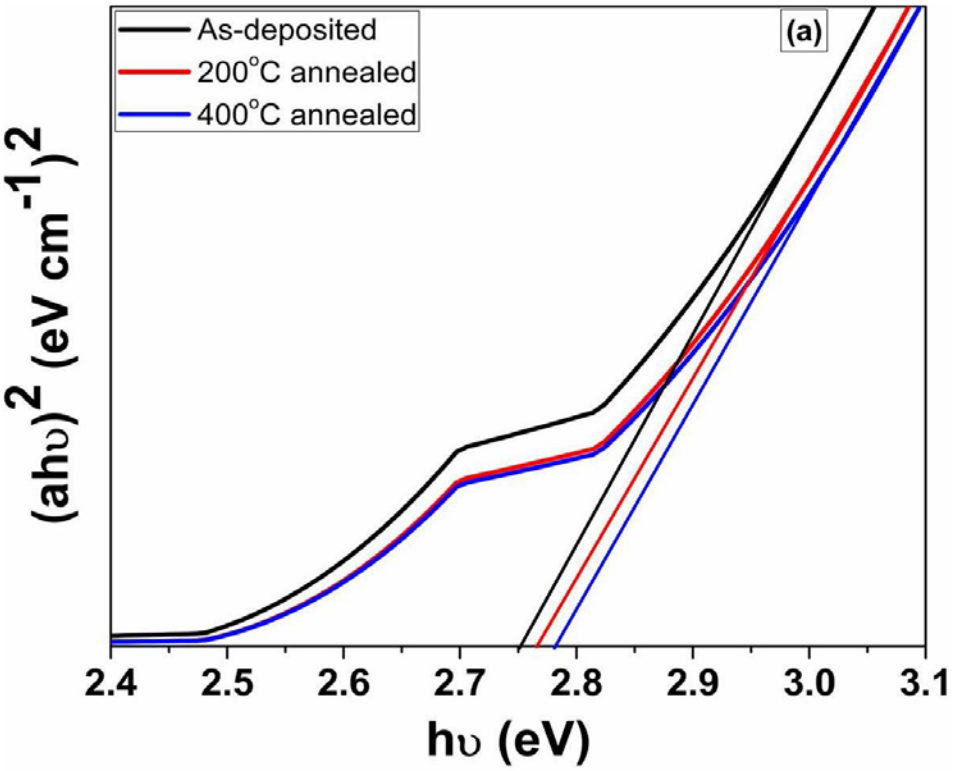

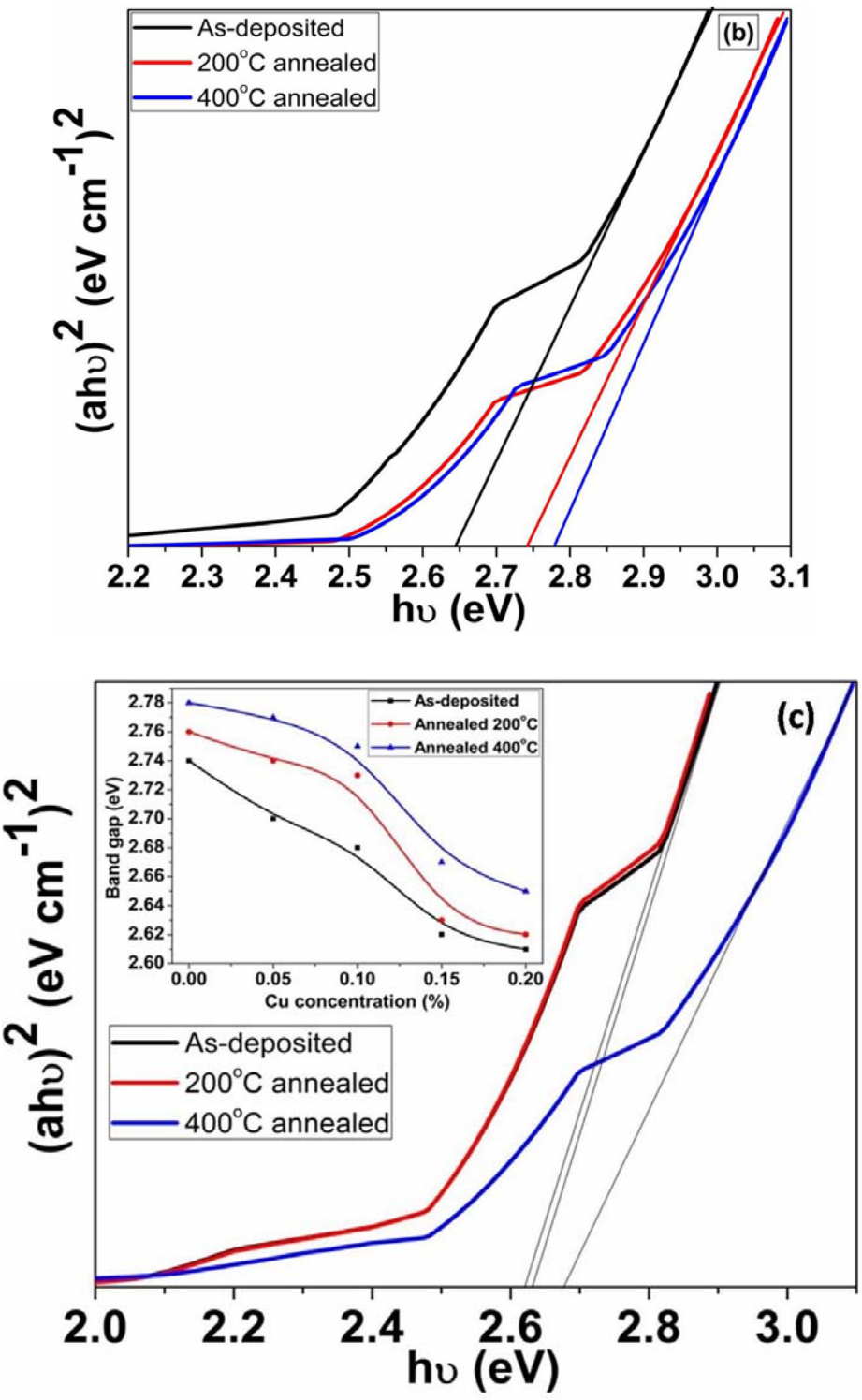

Fig. 4.10: Band gap energy of as-deposited and annealed (200ºC and 400ºC) $Zn_{1-x}Cu_xSe$ (a) x= 0.00, (b) x= 0.05, (c) x= 0.15 films, determined from k-spectra. Inset in Fig. 10c shows the variations of band gap energy of as-deposited and annealed (200ºC and 400ºC) $Zn_{1-x}Cu_xSe$ films with copper concentration.

Resulting from the fitting of the experimental data with the simulated one, the thickness of the deposited films is calculated for all samples and is listed in the table 4.1. The thicknesses of the $Zn_{1-x}Cu_xSe$ films were approximately 5% bigger than those calculated by the RBS. This variation in the thickness by the two spectroscopies is due to the diversity in the fitting software's and the mode of simulating the data. The complex dielectric function (ε_1) of $Zn_{1-x}Cu_xSe$ films obtained from the ellipsometery fit is shown Fig. 4.11(a-c).

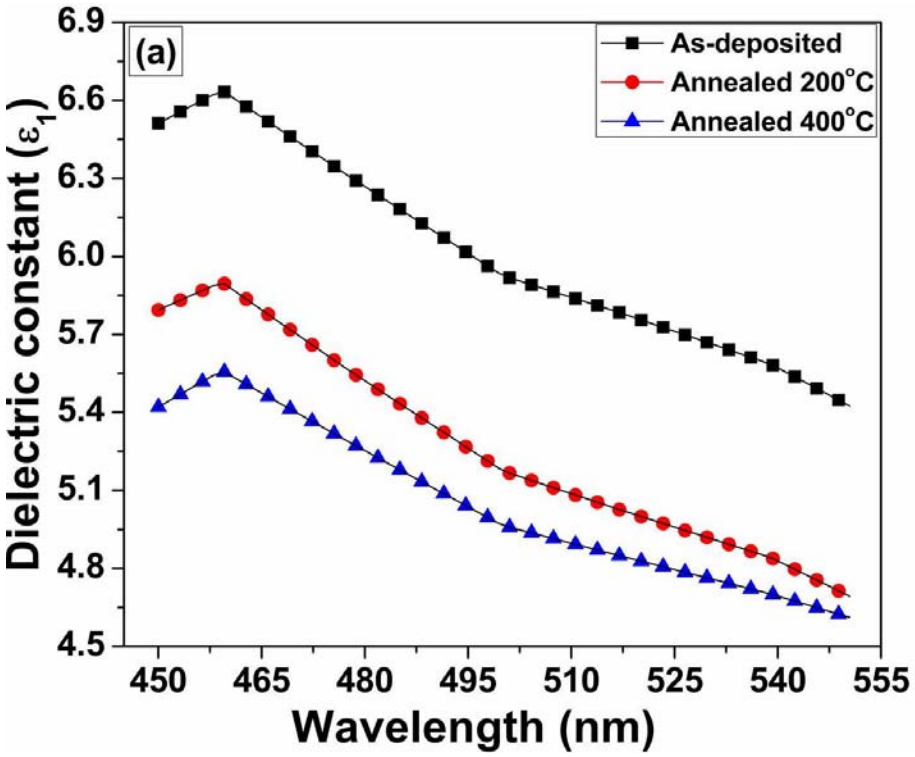

ε_1 is the real part of the complex dielectric function $\varepsilon=\varepsilon_1+i\varepsilon_2$ which correspond to how actually a material can be polarized whilst an electric field is applied due to formation of electric dipoles in the material. Change in the polarization of any material directly affects the dielectric properties of the material. This change in the dielectric constant is measured by the fitting of ellipsometery parameters psi (ψ) and delta (Δ). Ellipsometer measures the dielectric constant (ε_1) by the following equation [11].

$$\varepsilon_1=n^2 \qquad (10)$$

Where ‘n’ is the refractive index and is reported for the same as-deposited and annealed $Zn_{1-x}Cu_xSe$ films in the wavelength range 450-550 nm in another paper [12]. Fig. 4.11c shows that the dielectric constant (ε_1) values decreases with increasing annealing temperature. The average values of dielectric constant were found to vary between 5.42–4.61 (X=0) and 8.12–7.74 (X=0.20) for as-deposited and 400ºC annealed films respectively in the wavelength range of 450–550 nm. Post annealing of the deposited ZnSe films plays a vital role, which influences the dielectric properties of the deposited $Zn_{1-x}Cu_xSe$ films. The dielectric constant for 200ºC annealed film with 0% Cu concentration is found to be 4.69 at 550 nm wavelength which is 86% of the as-deposited film. The decrease in the dielectric constant with annealing temperature may be due to the lower density of annealed ZnSe films than as-deposited ZnSe films. Similar results have been reported for annealed ZnSe films [10,13]. The effect of annealing on the dielectric constant of all the as-deposited and annealed films at 550 nm wavelength is shown as an inset of Fig. 4.11c.

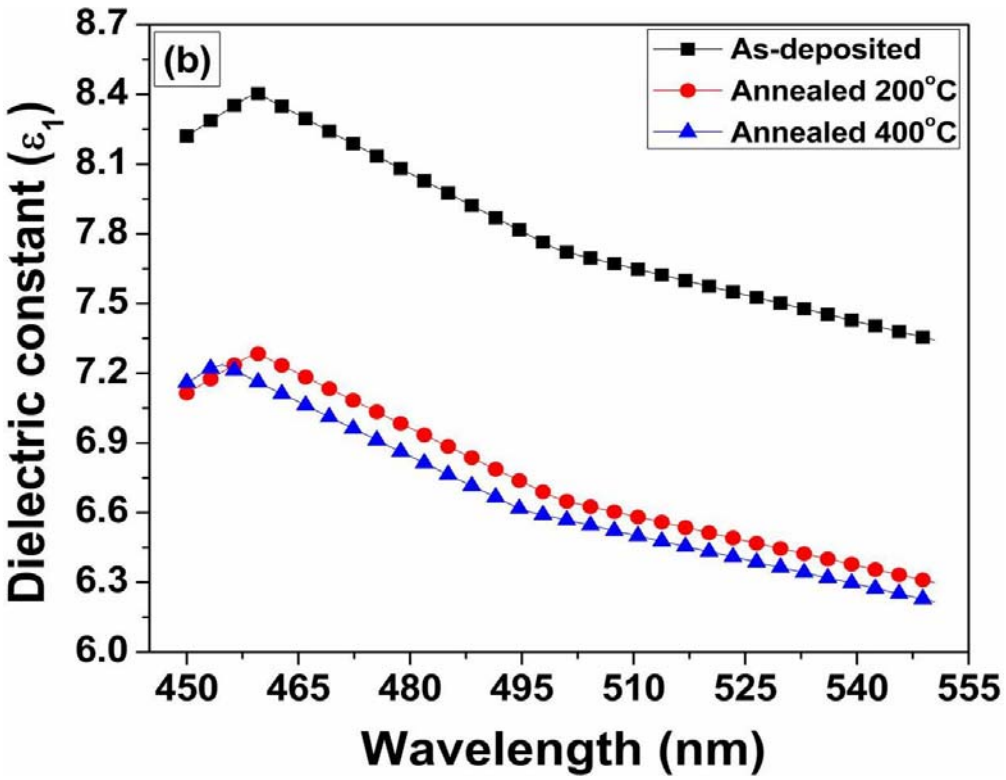

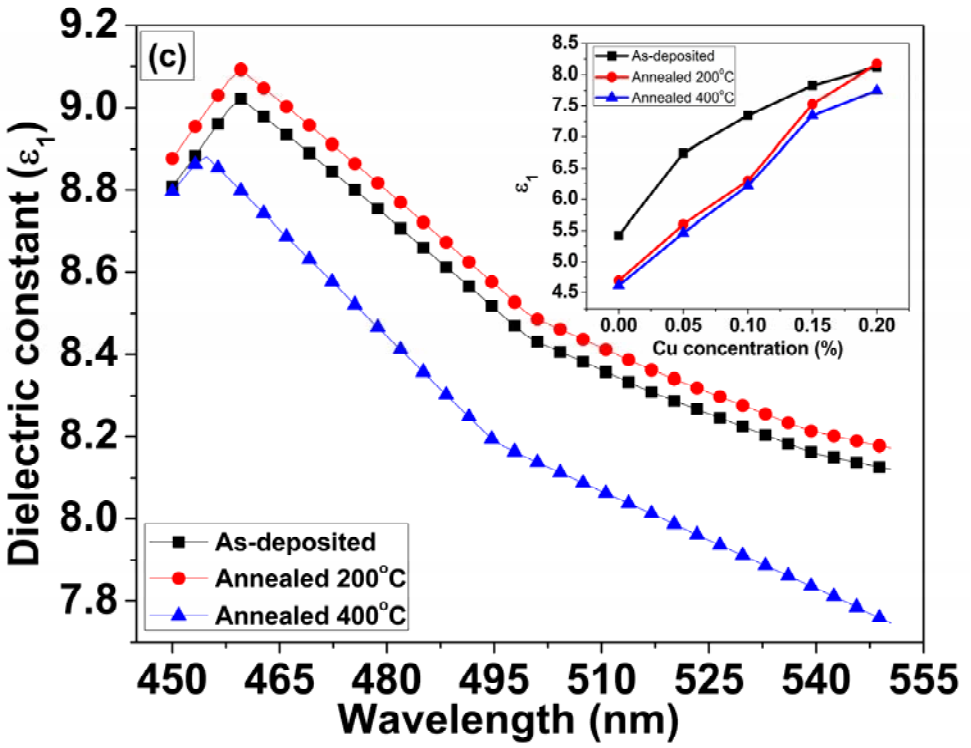

Fig. 4.11: Dielectric constant (ε_1) of as-deposited and annealed $Zn_{1-x}Cu_xSe$ (a) x=0.00 (b) x=0.05, (c) x=0.20 films, determined by spectroscopic ellipsometer. Inset in Fig. 4.11c shows the variations of dielectric constant of as-deposited and annealed (200°C and 400°C) $Zn_{1-x}Cu_xSe$ films with copper concentration at λ=550 nm.

4.4 References

1. L. R Doolittle. Algorithms for the rapid simulation of Rutherford backscattering spectra. Nuclear instruments and methods in Physics research section B: Beam interactions with materials and atoms 9 (1985) 344-351.
2. A. Kitahara, S. Yasuno, K. Fujikawa. Study of thin-film thickness and density by high-resolution Rutherford backscattering spectrometry and X-ray reflectivity. Trans. Mat. Res. Soc. Japan 34 (2009) 613-615.
3. P. K. R. Kalita, B. K. Sarma, H. C. Das. Structural characterization of vacuum evaporated ZnSe thin films. Bull Mater. Sci. 23 (2000) 313–7.
4. A. K. S. Aqili, A. Maqsood, Z. Ali. Appl. surf. Sci. 180, 73 (2001).
5. V. S. John, T. Mahalingam, J. P. Chu. Solid State Elect. 49, 3 (2005).

6. Jing-quan Zhang, Liang-huan Feng, Wei Cai, Jia-gui Zheng, Ya-ping Cai, Bing Li, Li-li Wu, Ye Shao. Thin Solid Films 414, 113 (2002).
7. V. Gupta, A. Mansingh. Influence of postdeposition annealing on the structural and optical properties of sputtered zinc oxide film. j. Appl. Phy. 80 (1996) 1063.
8. P. T. K. Chin, J. W. Stouwdam, R. A. J. Janssen. Nano Letters 9, 745 (2009).
9. D.A. Mazón-Montijo, M. Sotelo-Lerma, L. Rodríguez-Fernández, L. Huerta. AFM, XPS and RBS studies of the growth process of CdS thin films on ITO/glass substrates deposited using an ammonia-free chemical process. Appl. Surf. Sci. **256** (2010) 4280.
10. M. Arslan, A. Maqsood, A. Mahmood, A. Iqbal. Structural and optical properties of copper enriched ZnSe thin films prepared by closed space sublimation technique. Mat. Sci. Semicond. Proc. **16** (2013) 1797-1803.
11. R. P. Sharma, K. C. Sharma, J. C. Garg. Optical properties of $Cu_{3-x}InSe_2$ (0.8<or=x<or=2.3) films. J. Phys. D: Appl. Phys. **24** (1991) 2084.
12. J. Tauc. Amorphous & Liquid Semiconductors. Plenum, New York (1974) 159.
13. P. P. Hankare, V. M. Bhuse, K. M. Garadkar, A. D. Jadhav. A novel method to grow polycrystalline HgSe thin film. Mater. Chem. Phys. **71** (2001) 53-57.
14. J. Kvietkova, B. Daniel , M. Hetterich , M. Schubert , D. Spemann. Optical properties of ZnSe and $Zn_{0.87}Mn_{0.13}Se$ epilayers determined by spectroscopic ellipsometery. Thin Solid Films **455–456** (2004) 228-230.
15. R. Dahmani, L. Salamanca Riba, N. V. Nguyen, D. C. Horowitz, B. T. Jonker. Determination of the optical constants of ZnSe films by spectroscopic ellipsometery. J. Appl. Phys. **76** (1994) 514.
16. E. F. Schubert, J. K. Kim and J.-Q. Xi. Low-refractive-index materials: A new class of optical thin-film materials. phys. stat. sol. B. **244** (2007) 3002-3008.
17. M. Arslan, R. Muhammad, A. Mahmood, R. Rasheed. Effect of thermal annealing on the physical properties of $Zn_{1-x}Cu_xSe$ thin films deposited by close spaced sublimation technique. Acta Metall. Sin. (Engl. Lett.) **26** (2013) 699-706.
18. S. Venkatachalam, D. Soundararajan, P. Peranantham, D. Mangalaraj, S. K. Narayandass, S. Velumani, P. Schabes-Retchkiman. Spectroscopic ellipsometry (SE) studies on vacuum-evaporated ZnSe thin films. Materials Characterization **58** (2007) 715-720.

CHAPTER 5

5 CONCLUSIONS AND FUTURE RECOMMENDATIONS

5.1 Conclusions

The effect of post deposition thermal annealing on the compositional stoichiometry and depth concentration of deposited layers of $Zn_{1-x}Cu_xSe$ thin films was investigated by RBS technique. By increasing the annealing temperature of films from 200°C to 400°C the physical properties have improved significantly which shows that annealing effect is very prominent in the properties of thin films. The results attained from the RBS shows that the composition is intact in thin films while the thickness increases with increasing temperature. Variations in stoichiometry found with RBS technique is complemented by micro analysis characterization performed by XRD, AFM and the optical property results obtained using spectroscopic ellipsometer. XRD data predicts the enhancement of crystallinity with an increase in FWHM value while stacking fault energy decreases with increasing annealing temperature. AFM suggests the formation of very smooth surface. It is observed that surface roughness (RMS) increases from 1.1118 nm to 1.3893 nm for x= 0.00 to 0.10 as-deposited films respectively with increase of Cu concentration. Spectroscopic ellipsometery analysis reveals that the bang gap increases while dielectric constant decreases with the increase in annealing temperature.

5.2 Future Recommendations

Pursuant to the reported literature, ZnSe has become much promising material in optoelectronic device appliances, especially in the UV region [1-8]. At present some of the II-VI compound semiconductors are being used as buffer layers for the fabrication of solar cells. For example CdS [10], CdTe [11] and CIGS [12] are the most widely used buffer layer materials for solar

cells fabrication, but due to the harmful nature of these materials much consideration has been focused on developing toxic free layers. One such alternate is ZnSe because it is environment friendly as well as it has wide band gap (2.7eV) as compared to above mentioned materials. Moreover, ZnSe based solar cells has an efficiency greater than 11% by transmitting higher energy photons to the absorber layer of the solar cell [13-14] therefore, it can be used as a buffer and window layer in the solar cells.

Since most electronic devices are manufactured in the shape of thin films, the film fabrication and characterization plays a fundamental role in the applications of semiconductor technology. Although the ZnSe thin films have been extensively studied, preparation of copper doped zinc selenide and its characteristics have not been reported with greater concentrations of copper. In the present work, study of physical properties of copper doped zinc selenide thin films using ZnSe and copper as precursors has been studied. For future research suggestions, other dopant concentrations of comparable physical properties can be enriched in ZnSe matrix to obtain enhanced properties particular for device fabrication. Furthermore, effect of annealing has been discussed in detail for all the deposited films. For annealing treatment, different methods can be adopted, such as for semiconducting films thermal annealing and laser annealing can be used. Also different Parameters such as annealing time, atmosphere, temperature and pressure could be varied to obtain better and optimum optical and structural properties.

According to my knowledge the effects of thermal annealing on the compositional, structural and optical properties of the $Zn_{1-x}Cu_xSe$ films have been investigated and discussed for the first time with greater concentrations of copper. We can use other deposition techniques for the deposition of $Zn_{1-x}Cu_xSe$ films for entirely new properties. In order to acquire specific knowledge of the structural and optical properties about thin films, one has to keep the exact composition and stoichiometry of the fabricated film layers especially for designing modern optoelectronic and optical devices. Irrespective of the deposition technique, deep analysis of the microstructure and morphology fruition in polycrystalline ZnSe films is of key significance to develop a clear understanding of the performance of devices employing these layers. In the present study, we demonstrated several results of the RBS analysis of the deposited films using high-energy 2 MeV He^+ ion beams from a pelletron tandem-type ion accelerator. Other methods for the quantitative and qualitative information about stoichiometry and establishment of interfaces doped

semiconductor as a function of depth or dopant specie can also be studied. These methods include particle induced X-ray emission (PIXE) or X-ray protoelectron spectroscopy (XPS).

5.3 References

1. O. Schulz, M. Strassburg, T. Rissom, U.W. Pohl, D. Bimberg.Appl. Post-growth *p*-type doping enhancement for ZnSe-based lasers using a Li_3N interlayer. Phys. Lett. **81** (2002) 4916.
2. P. Mahawela, G. Sivaraman, S. Jeedigunta, J. Gaduputi, M. Ramalingam, S. Subramanian. II–VI compounds as the top absorbers in tandem solar cell structures. Mater. Sci. Eng. B. **116** (2005) 283.
3. P.K. Kalita, B.K. Sarma, H.L. Das. Structural characterization of vacuum evaporated ZnSe thin films. Bull. Mater. Sci. **23** (2000) 313.
4. S. Venkatachalam, S. Agilan, D. Mangalaraj, S.K. Narayandass. Optoelectronic properties of ZnSe thin films. Mater. Sci. Semicon. Proc. **10** (2007) 128.
5. Xiaojun Zhang, Kin Man Yu, Coleman X. Kronawitter, Zhixun Ma, Peter Y. Yu, andSamuel S. Mao. Heavy p-type doping of ZnSe thin films using Cu_2Se in pulsed laser deposition. Appl. Phys. Lett. **101** (2012) 042107.
6. T. Shi rakawa. Effect of defects on the degradation of ZnSe-based white LEDs. Mater. Sci. Eng. B **91-92** (2002) 470.
7. M. Godlewski, E. Guziewicz, K. Kooalko, E. Lusakowska, E. Dynowska, M.M. Godlewski, E.M. Godys, M.R. Phillips. Origin of white color light emission in ALE-grown ZnSe. J. Lumin. **102–103** (2003) 455.
8. M. Drechsler, B.K. Meyer, D.M. Hofmann, P. Ruppert, D. Hommel. Optically detected cyclotron resonance properties of high purity ZnSe epitaxial layers grown on GaAs. Appl. Phys. Lett. **71** (1997) 1116.
9. S. Venkatachalam, D. Mangalaraj, Sa. K. Narayandass, K. Kim, J.Yi. Structure, optical and electrical properties of ZnSe thin films. Physica B **358** (2005) 27–35.

10. S. Kumazawa, S. Shibutani, T. Nishio, T. Aramoto, H. Higuchi, T. Arita, A. Hanafusa, K. Omura, M. Murozono, H. Takakura. 15.1% Highly efficient thin film CdS / CdTe solar cell. Solar Energy Materials and Solar Cells **49** (1997) 205–212.

11. N. Romeo, A. Bosio, V. Canevari, A. Podesta. Recent progress on CdTe/CdS thin film solar cells. Characteristics of Cu(In,Ga)Se_2 (CIGS) thin films deposited by a direct solution coating process. Solar Energy. **77** (2004) 795–801.

12. M. G. Park, S. Ahn, J. H. Yun, J. Gwak, A. Cho, S. Ahn, K. Shin, D. Nam, H. Cheong, K. Yoon. J. Alloys and Comp. **513** (2012) 68–74.

13. A. Ennaoui, S. Siebentritt, M. Ch. Lux-Steiner, W. Riedl, F. Karg. High-efficiency Cd-free CIGSS thin-film solar cells with solution grown zinc compound buffer layers. Sol. Energy Mater. Sol. C **67** (2001) 31–40.

14. W. Eisele, A. Ennaoui, P. Schubert-Bischoff, M. Giersig, C. Pettenkofer, J. Krauser, M. Lux-Steiner, S. Zweigart, F. Karg. XPS, TEM and NRA investigations of Zn(Se,OH)/$Zn(OH)_2$ films on Cu(In,Ga)$(S,Se)_2$ substrates for highly efficient solar cells**.** Sol. Energy Mater. Sol. C **75** (2003) 17–26.